ADVANCED MODULATION FORMATS AND ALL-OPTICAL PROCESSING SOLUTIONS FOR FUTURE FIBER-OPTIC COMMUNICATION SYSTEMS

By

Hacène Mahieddine Chaouch

A Dissertation Submitted to the Faculty of the

College of Optical Sciences

In Partial Fulfillment of the Requirements
For the Degree of

DOCTOR OF PHILOSOPHY

In the Graduate College

THE UNIVERSITY OF ARIZONA

2011

THE UNIVERSITY OF ARIZONA
GRADUATE COLLEGE

As members of the Dissertation Committee, we certify that we have read the dissertation prepared by:

Hacene Mahieddine Chaouch

entitled:

Advanced Modulation Formats and All-Optical Processing Solutions for Future Fiber-Optic Communication Systems

and recommend that it be accepted as fulfilling the dissertation requirement for the Degree of **Doctor of Philosophy**

_**Dr. Franko Kueppers**_____Date: 30/11/2011

_**Dr. Carl Maes**_____Date: 30/11/2011

_**Dr. Matthew Kupinski**_____Date: 30/11/2011

Final approval and acceptance of this dissertation is contingent upon the candidate's submission of the final copies of the dissertation to the Graduate College.

I hereby certify that I have read this dissertation prepared under my direction and recommend that it be accepted as fulfilling the dissertation requirement.

_____ Date: 30/11/2011
Dissertation Director: **Dr. Franko Kueppers**

_____ Date: 30/11/2011
Dissertation Director: **Dr. Carl Maes**

STATEMENT BY AUTHOR

This dissertation has been submitted in partial fulfillment of requirements for an advanced degree at the University of Arizona and is deposited in the University Library to be made available to borrowers under rules of the Library.

Brief quotations from this dissertation are allowable without special permission, provided that accurate acknowledgment of source is made. Requests for permission for extended quotation from or reproduction of this manuscript in whole or in part may be granted by the head of the major department or the Dean of the Graduate College when in his or her judgment the proposed use of the material is in the interests of scholarship. In all other instances, however, permission must be obtained from the author

SIGNED: Hacene Chaouch

ACKNOWLEDGEMENTS

I would like first to thank my advisor Prof. Franko Kueppers who believed, from the beginning, in my ability to do research in his group and who encouraged and supported me in all my endeavors. His commitment towards students is simply unique.

I would like also to address a special thank to Dr. Earl Parsons. Doing research with Earl was an exciting day-to-day experience.

Finally, many thanks to Dr. Tuomo von Lerber, Dr. Sascha Vorbeck, Dr. Werner Weiershausen, and Dr. Malte Schneiders for their support and help in my research, internships and job search.

DEDICATION

To my parents Athmane and Malika Chaouch who taught me from a very young age to love and respect knowledge

To my sister Halla who always prayed for me throughout the good and tough times

To my sisters Amina, and Amel and my brother Ahmed who always pushed me to do better.

TABLE OF CONTENTS

LIST OF FIGURES

CHAPTER 1

CHAPTER 2

CHAPTER 3

CHAPTER 4

LIST OF TABLES

ABSTRACT

In this dissertation we present the research findings around two important hot topics of modern and future fiber-optic communication systems: 100 Gbit/s transmission and all-optical processing of received phase-modulated signals.

The findings are discussed in the same chronological order they were obtained.

Each topic is summarized in two chapters that correspond to one selected journal and one conference publications.

The first and second chapters are dedicated to the simulation and numerical analysis of 100 Gbit/s systems.

In chapter one, we present a thorough investigation of the best 100 Gbit/s serial modulation format. Seven different modulation formats are considered and are compared in terms of tolerance to dispersion and maximum reach for a 10^{-9} bit error rate target.

In chapter two, the behavior of chapter one's best candidate is analyzed in a realistic environment. The influence of the existing lower data rate neighboring channels is discussed in particular. The results of these two chapters were obtained in collaboration with engineers from the Deutsche Telekom Technology Center in Darmstadt, Germany. They served as a theoretical basis for a field trial carried out by this same company.

Chapter three and four focus on the use of semiconductor optical amplifiers for all-optical processing applications. Impaired phased-modulated signals are under particular interest in this study. The novelty in this work resides in the counter-propagating configuration that the semiconductor optical amplifier is operated in.

In chapter three we give a detailed description of the experimental results. The complete setup is explained and the improvement in Q-factor and bit error rate for the received signal is proven. Furthermore, two novel concepts (Photonic Balancing and Saturated Asymmetric Filtering) that explain the observed improvements are developed and discussed for the first time to the best of our knowledge.

Finally, chapter four aims at optimizing numerically the experimental setup for the saturated asymmetric filtering technique. The required detuned filter after the saturated semiconductor optical amplifier is optimized in terms of both off set and bandwidth.

CHAPTER 1

NUMERICAL ANALYSIS AND SYSTEM OPTIMIZATION FOR 100 GBIT/S CARRIER ETHERNET SERIAL MODULATION FORMATS

1.1 Introduction

In recent years, the public demand for broadband internet access has grown strongly, fueling the exponential increase of internet traffic. Besides broadband internet access, new high-definition video services along with business customers needs constitute nowadays the key driver for further increasing bandwidth demand. Indeed this demand extends the current broadband leased lines (based on circuit switched Layer 1 peer-to-peer and/or virtual private networks) by using dedicated high-speed Optical Transport Hierarchy and Wavelength Division Multiplexing (OTH/WDM) channels.

To support this high bandwidth demand, network operators and service providers need to upgrade their access, aggregation, and core networks. Although some network operators have started to deploy 40 Gbit/s dense wavelength division multiplexing (DWDM) systems, the 100 Gbit/s carrier grade Ethernet technology is already considered a reasonable alternative for a large scale system roll-out of next generation DWDM networks [1,2]. Hence, 100 Gbit/s interface line rates are being already standardized for high-speed Ethernet and for efficient internet protocol (IP) router interconnection applications and will probably be introduced in the mid 2010.

Consequently, a request for long-haul transport supporting this logical interface format will follow as the next step. Besides the purely serial on-off-keying (OOK) transmission

solution, multi-level phase shift keying modulation formats (e.g. DQPSK) or inverse multiplexing of several parallel lower-speed DWDM channels (e.g. 10×10 Gbit/s) may be applied. Moreover, the decision-making process will be mainly dominated by investment costs: transponder complexity and fiber link utilization efficiency. This last requirement includes a high spectral efficiency as well as significant, optically transparent, transmission distances; both of which need to be studied and characterized for all possible modulation format candidates.

This chapter investigates numerically the performance of different 100 Gbit/s single-channel serial transmission solutions. They are eventually compared to the alternative inverse multiplexing concept based on a standard 10 Gbit/s per wavelength DWDM scheme. Note that the inverse multiplexing scheme differs from the classical demultiplexing technique in that each of the 10 Gbit/s channels contains a part of the same 100 Gbit/s data stream. Various amplitude shift keyed (ASK) and phase shift keyed (PSK) modulation formats are compared in terms of chromatic dispersion tolerance and system reach under specific conditions representative for real networks. For the first time, to the best of our knowledge, the system reach tolerance (of five different formats) with respect to variations of the single mode fiber (SMF) and dispersion compensating fiber (DCF) input powers is characterized for a fixed 10^{-9} BER target. Optical Raman amplification and electronic forward error correction (FEC) are not considered in this study. The compared modulation formats include:

- Non-return-to-zero, NRZ;
- Return-to-zero, RZ, with various duty cycles;
- Carrier-suppressed-return-to-zero, CS-RZ;
- Differential (quaternary) phase shift keying, NRZ-D(Q)PSK and RZ-D(Q)PSK;
- Optical duobinary, ODB;
- Non-return-to-zero vestigial sideband, NRZ-VSB;
- 10×10 Gbit/s NRZ (DWDM).

1.2 Simulation Setup and Parameters

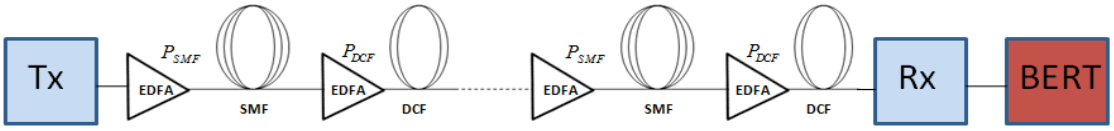

Fig. 1. Block diagram of the simulated set-up using the following fiber parameters:
α_{SMF} = 0.21 dB/km, D_{SMF} = 17 ps/nm/km, ΔD_{SMF} = 0.056 ps/nm^2/km, γ_{SMF} = 1.317 1/W/km
α_{DCF} = 0.5 dB/km, D_{DCF} = -100 ps/nm/km, ΔD_{DCF} = -0.3294 ps/nm^2/km, γ_{DCF} = 5.27 1/W/km
(α: attenuation, D: chromatic dispersion, ΔD: dispersion slope, γ: nonlinear coefficient).

The simulated system set-up is shown above in Fig. 1. A transmitter block (Tx, PRBS 2^{10}-1) is followed by the first – 100% post-compensated – span of the transmission line consisting of an erbium-doped fiber amplifier (EDFA) with a noise figure (NF) of 5 dB. After the EDFA an amplified optical signal with an average power P_{SMF} is launched into the transmission fiber. A separate EDFA with the same NF is used to control the power launched into the dispersion compensating fiber (DCF), P_{DCF}. The receiver block (Rx) includes a 100 GHz bandwidth 1st order Gaussian optical filter aimed to remove the out

of band noise. One or two delay interferometers are used for optical demodulation in the case of (N)RZ-DPSK and (N)RZ-DQPSK formats, respectively. Finally, balanced detection with electrical (1st order Bessel function) filtering is used to detect the signal. An eye analyzer (EA) provides the eye opening (EO) of the received signal.

For ASK formats, BERs are estimated using an analytical bit error rate tester (BERT). This analytical BERT calculates the BER from the received Q-factor based on a Gaussian approximation of the optical noise. Although the actual noise distribution is not exactly Gaussian, this method has been demonstrated to give accurate results for low BERs [3, 4] and offers therefore an alternative to the prohibitive time-consuming direct bit error counts. In the special case of intensity modulated signals (IM) the BER is thus given by

$$Q = \frac{\mu_1 - \mu_0}{\sigma_1 + \sigma_0} \quad ; \quad BER(Q) = \frac{1}{2} erfc(\frac{Q}{\sqrt{2}}) \tag{1}$$

Where $\sigma_{1,0}$ and $\mu_{1,0}$ are the standard deviation and the mean of the transmitted logical "one" or "zero", and erfc is the complementary error function. A more comprehensive mathematical description can be found in [5].

On the other hand, a fully numerical method based on the tail extrapolation algorithm was chosen for estimating BERs for PSK formats that are affected by the nonlinear phase noise present over such distances. Indeed, a direct estimation of the BER from the Q-factor can provide in this case inaccurate results, mainly due to the fundamentally non-Gaussian nature of the optical noise in this case, as demonstrated in [6].

1.3 Dispersion Tolerances

When considering such high bit rates, dispersion becomes a serious limitation that network providers have to deal with. Therefore, despite of its deterministic nature, it's particularly important to know precisely the chromatic dispersion compensation (CDC) for each format. In order to estimate the dispersion tolerances (DT), a single-span with only one EDFA (in front of the SMF) and with the DCF length varied in small steps, is compared to a back-to-back scheme. We use the eye opening penalty (EOP) parameter to evaluate the DT of each format since only the CD is considered here without the noise influence. The DT is taken as the region of accumulated dispersion where the EOP remains smaller than 1 dB. Accumulated dispersion here means the total residual dispersion accumulated by the signal while propagating through both the SMF and the DCF fibers. Fig. 2 (a) presents the evolution of the EOP with respect to the accumulated dispersion for all the mentioned ASK formats. Whereas Fig. 2 (b) shows in the same way this evolution for different PSK formats.

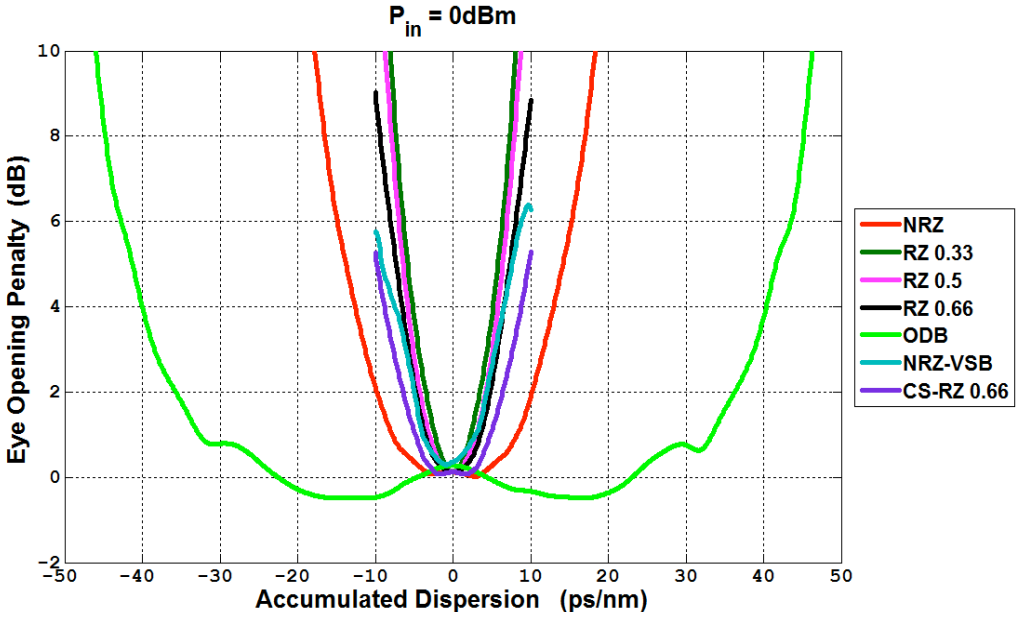

(a)

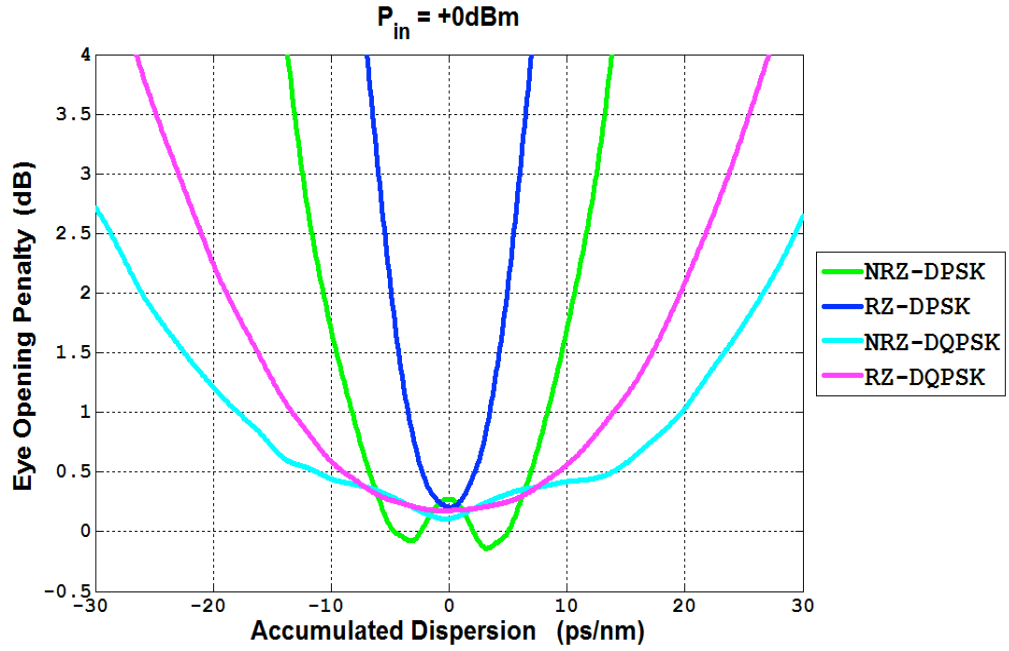

(b)

Fig. 2. EOP vs accumulated dispersion for different (a) ASK formats, (b) PSK formats

Fig. 2 (a) and (b) show the expected trends. Indeed, the EOP increases faster for formats with a broader spectrum, both for ASK and PSK schemes. In addition we see that the ODB format outperforms the whole group due to its very narrow spectrum. Fig. 3 shows as a result the DT taken at 1 dB EOP as mentioned previously. We see that the most tolerant formats are the ODB, NRZ-DQPSK and RZ-DQPSK with an approximate 66, 38 and 27 ps/nm DT respectively.

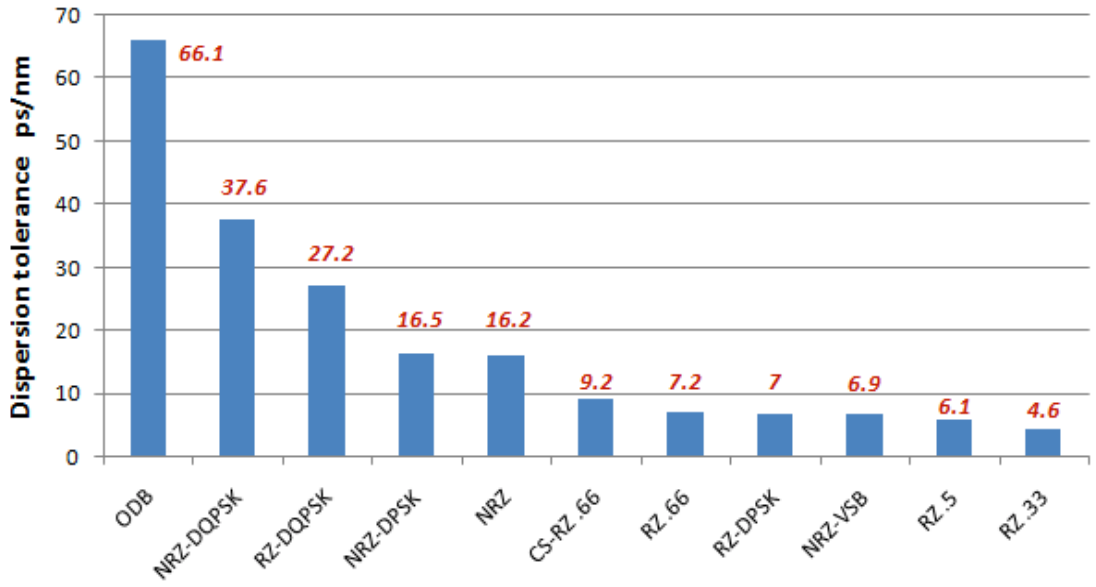

Fig. 3. Dispersion tolerances at 100 Gbit/s serial transmission for all ASK and PSK formats.

It's also important to notice that the (N)RZ-DQPSK scheme, strong of its halved symbol rate, is the most tolerant PSK format to dispersion. Indeed, the DT increases with decreasing symbol rate making the (N)RZ-DQPSK very attractive for 40→100 Gbit/s upgrade for the many existing routes initially designed for 10 Gbit/s. Finally, the 10×10 Gbit/s (DWDM) NRZ scheme with a 50 GHz channel spacing (see Table 1 of section 4) benefits of a much higher DT with an approximate 1400 ps/nm, but suffers from a significant operational complexity in addition to a very low spectral efficiency.

Fig. 2 was obtained while keeping the input power into the span relatively low (0 dBm as indicated on the top of this figure) so that we can neglect the influence of nonlinearities. It's important nevertheless to evaluate the robustness of the investigated DT for an increasing input power. Fig. 4 presents the evolution of the DT with respect to the launched input power for the considered ASK and PSK formats.

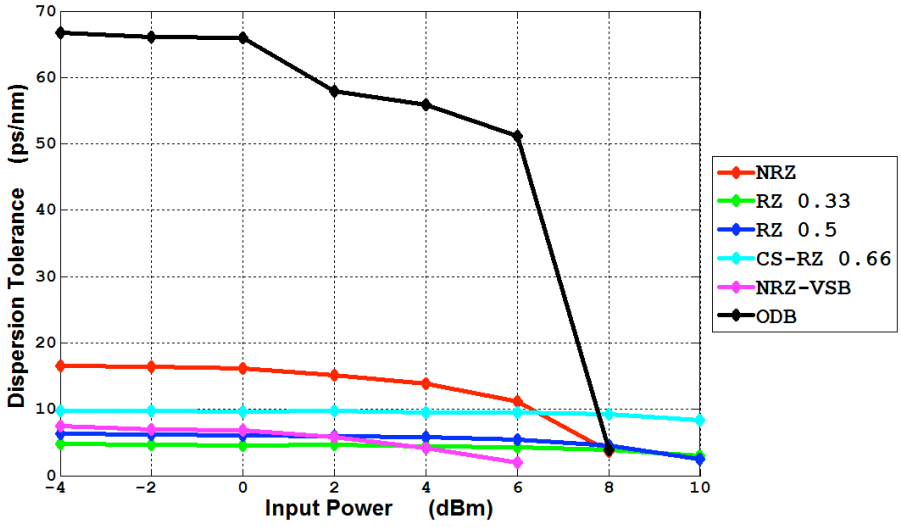

(a)

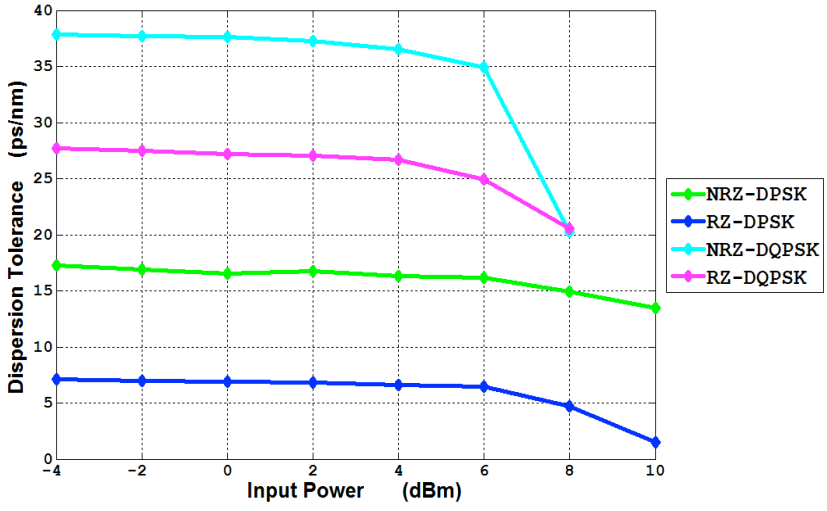

(b)

Fig. 4. Evolution of the dispersion tolerance over one span for different (a) ASK formats, (b) PSK formats with respect to the launched input power

Although the ODB format holds the highest DT for low input powers, Fig. 4 (a) shows that it has the steepest decline for input powers higher than 6 dBm, making it the format that suffers the most of nonlinearities. On the other hand the (N)RZ-DQPSK formats appear to be the most robust with a DT kept above 20 ps/nm over the range [-4, +8] dBm. The halved symbol rate that benefits this format is behind this robustness. Finally, as the nonlinearities are more critical for higher number of spans, these last formats would also constitute good candidates from a system reach perspective as shown in the next section.

1.4 System Reach

The maximum system reach is defined as the transmission length for which the BER is $\leq 10^{-9}$. For ASK formats the BER is calculated directly from the obtained Q-factor. On the other hand, a fully numerical method based on tail extrapolation algorithm, first introduced in [7], was chosen for the considered PSK formats mainly limited by the nonlinear phase noise. In fact, 10 blocks of 1024 bits each were simulated to obtain BER estimates in reasonable times.

The tail extrapolation algorithm provides very low BERs from fewer simulated bits, typically 10^4, 10^5 bits. A low BER corresponds to a low likelihood for an error to occur; this information being contained in the tail of the probability density, the extrapolation approach is to deduce the tail evolution from the center of the probability density function (PDF) where high error occurrences can be detected. To realize this extrapolation, we assume that the marks' and spaces' PDFs have a generalized exponential shape described by (2)

$$p_x(x) = \frac{\delta}{2\sqrt{2}\Gamma(\frac{1}{\delta})\varepsilon} \exp\left[-\left|\frac{x-m_x}{\sqrt{2}\varepsilon}\right|^{\delta}\right] \tag{2}$$

Where Γ is the gamma function and ε, δ are fitting parameters for a least square fit. The BER is then given by (3)

$$BER = \int_S^{\infty} p_x(x)dx \approx \exp\left[-\left(\frac{S-m_x}{\sqrt{2}\varepsilon}\right)^{\delta}\right] \tag{3}$$

S being the decision threshold that determines whether the bit is a logical 1 or 0.

In order to find the optimum BER estimate, S is swept over the actual bit error counts range. For every position, the BER is calculated by counting the number of errors and the optimum one is extrapolated using, first, (2) to deduce the best PDF fit and then (3) to solve for the minimum BER value. Fig. 5 (a) presents the balanced detected in-phase (I) eye diagram after demodulation of a100 Gbit/s RZ-DQPSK channel after five spans. Fig. 5 (b) shows the log(BER) evolution when the threshold is swept over the eye range. After extrapolation, the optimum BER corresponds to the intersection of the gray and the green curves.

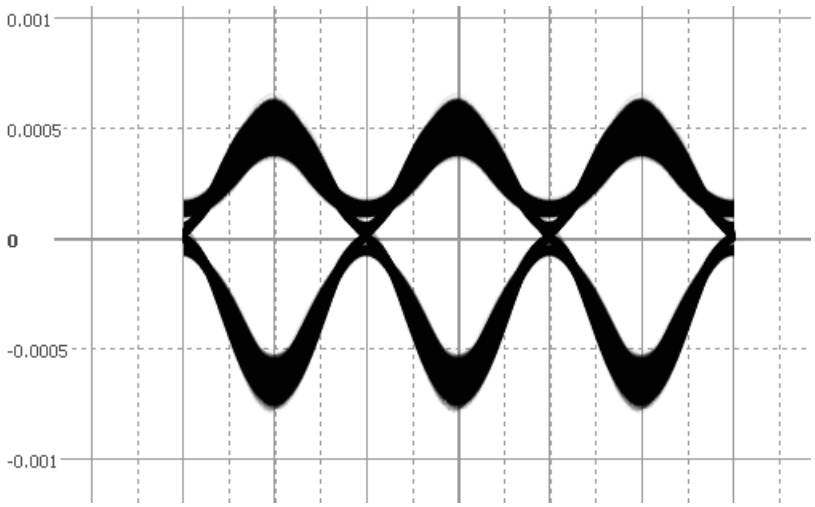

(a)

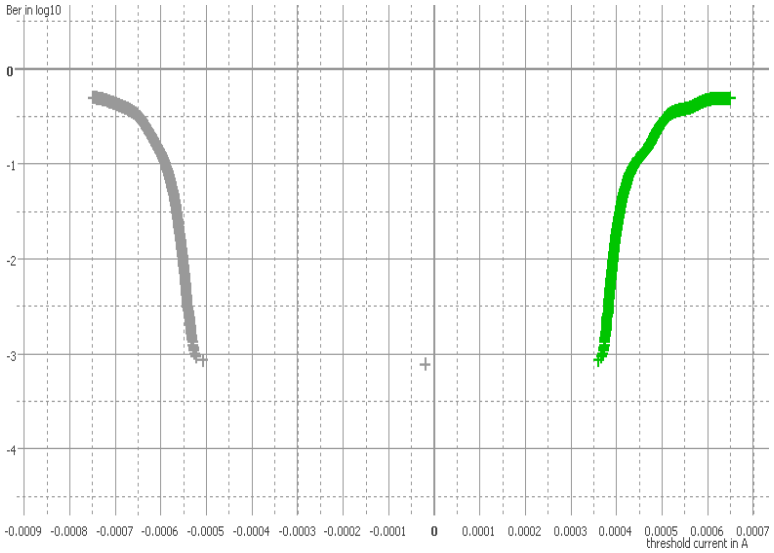

(b)

Fig. 5 (a) Eye diagram after balanced detection at the receiver side, (b) log(BER) evolution for different threshold values.

.

The SMF and DCF input power levels are varied in order to find the optimum balance between limitations due to noise and due to fiber nonlinearities. The results are presented in Fig. 6 for the two best ASK formats: RZ with 0.5 and CS-RZ with 0.66 duty cycles respectively. Fig. 7 shows, on the other hand, the two leading PSK formats RZ-DPSK and RZ-DQPSK whereas Fig. 8 and Fig. 9 present, respectively, the 10×10 NRZ (DWDM) scheme over SMF and the RZ-DQPSK one over NZDSF fiber type.

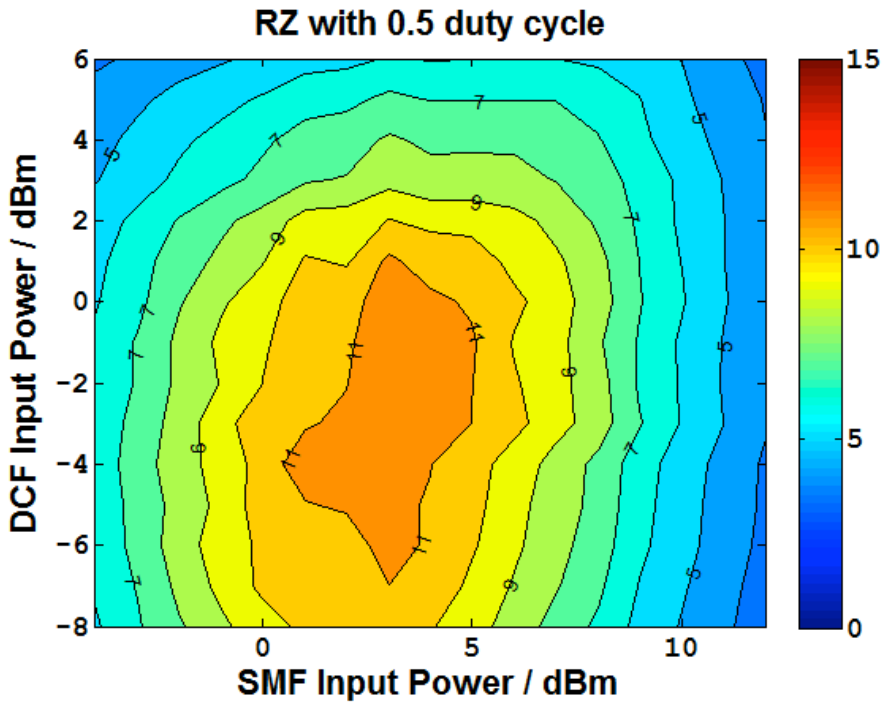

(a)

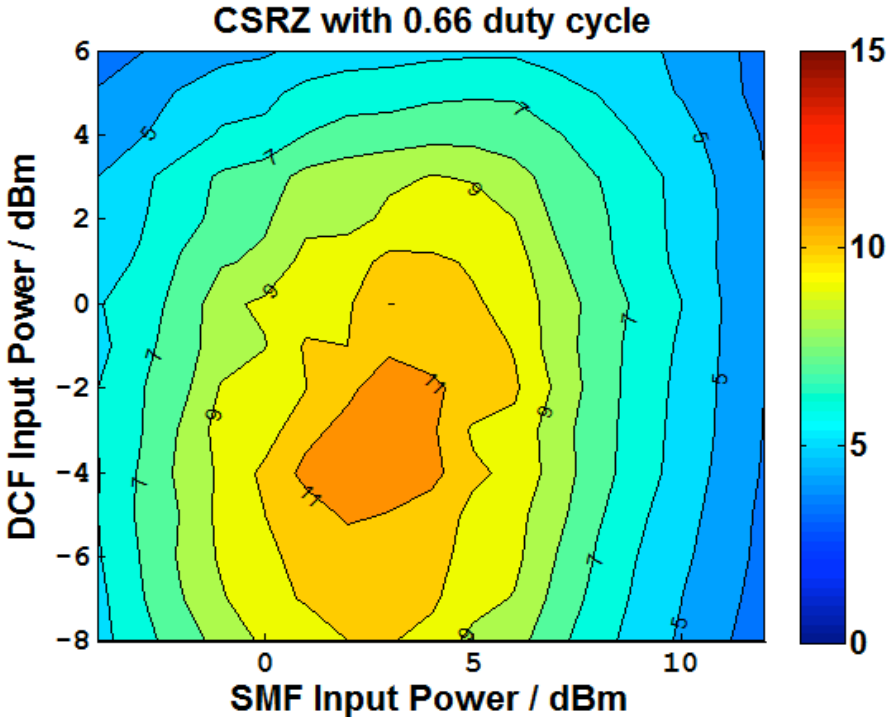

(b)

Fig. 6. System reach of the two best ASK formats for a 10^{-9} BER target. (a) RZ 0.5, (b) CSRZ 0.66. Note that the third dimension corresponds to the number of spans.

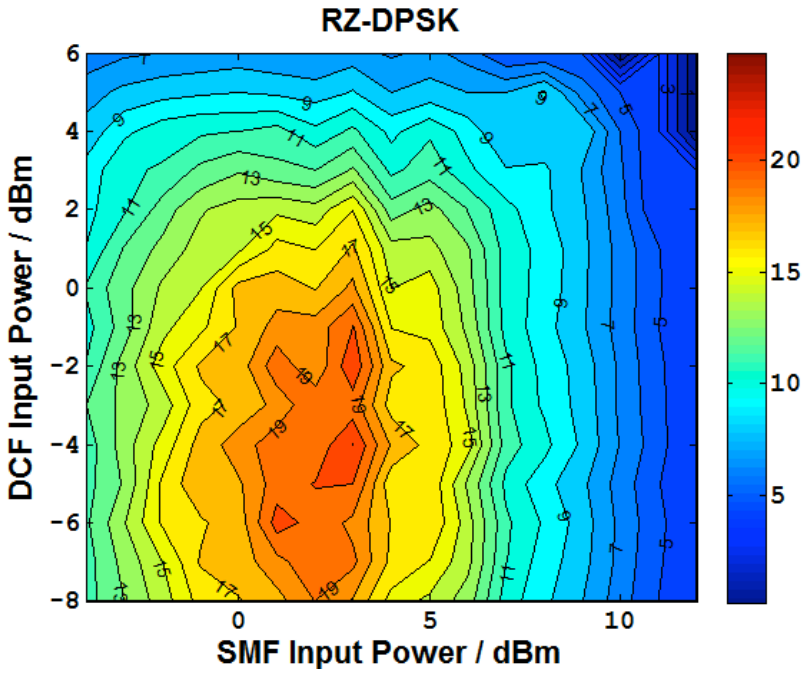

(a)

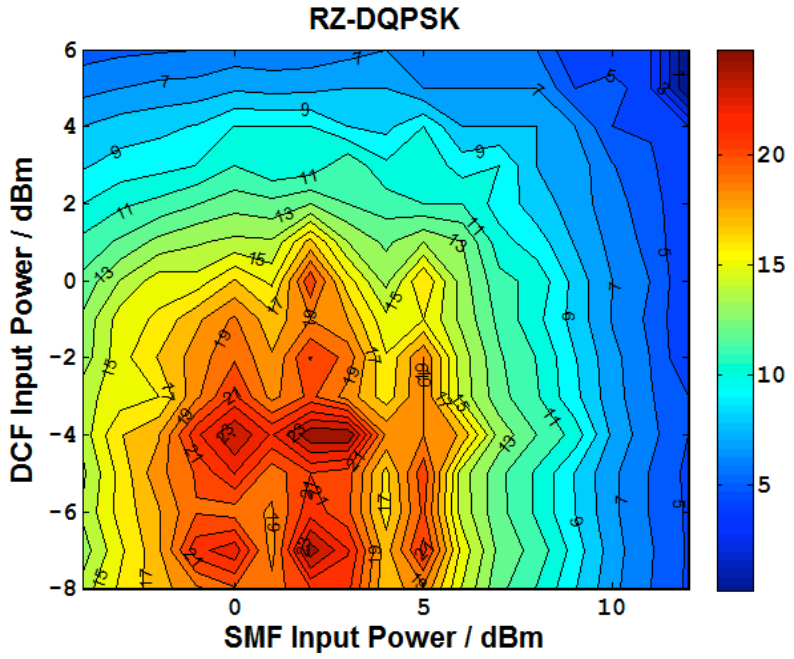

(b)

Fig. 7. System reach of the two best PSK formats for a 10^{-9} BER target. (a) RZ-DPSK , (b) RZ-DQPSK

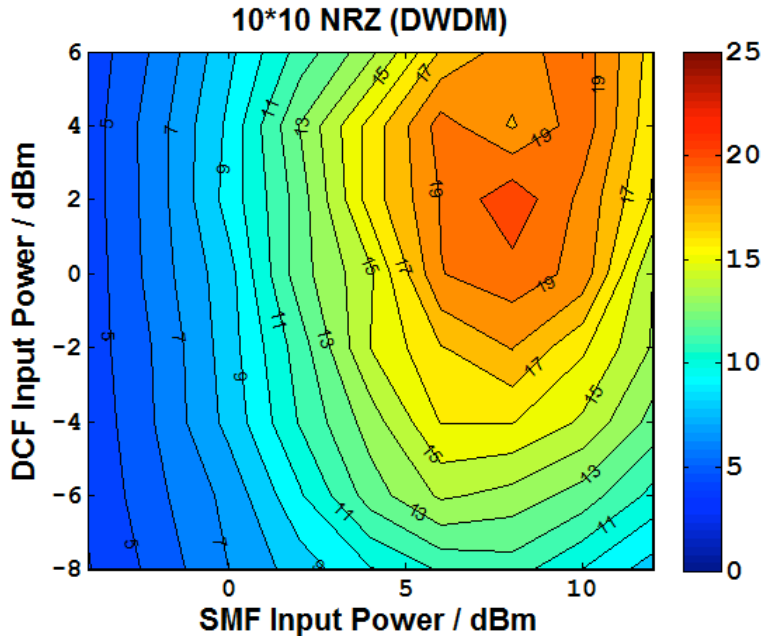

Fig. 8. System reach of the 10×10 NRZ (DWDM) scheme for a10^{-9} BER target. Note that the SMF and DCF input powers accumulated numbers for 10 channels. A simple power shift of -10 dB gives the corresponding power per channel.

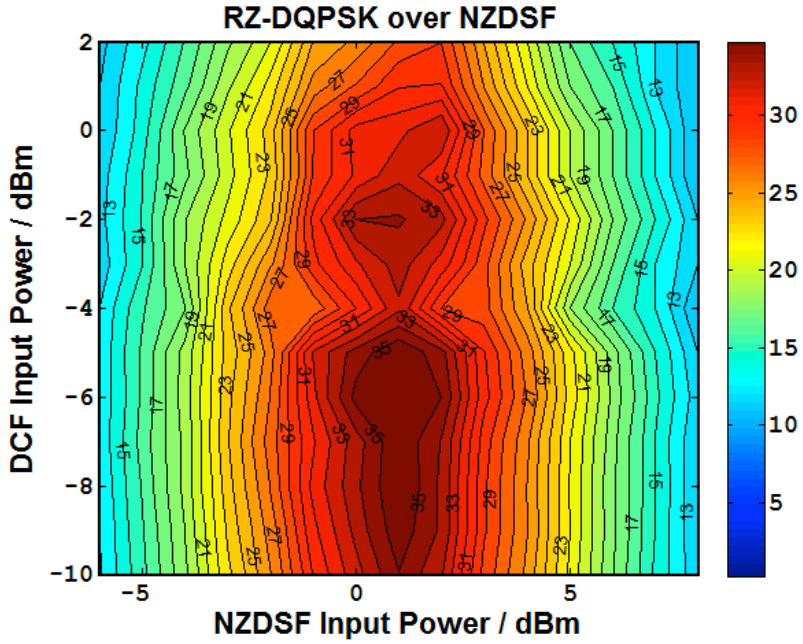

Fig. 9. System reach of the RZ-DQPSK modulation format using NZDSF also for a 10^{-9} BER target.

An important observation from Fig. 6, 7 is the fact that for a given targeted communication distance, the RZ-DPSK and RZ-DQPSK formats give much more input

power tolerance than the RZ and CS-RZ schemes. Indeed, if we consider a targeted distance of 10 spans (800 km), the RZ and CS-RZ formats' plots show an SMF input power range of [1,4] dBm and a DCF one of [-6,1] dBm and [-5,-2] dBm, respectively, for these two ASK formats. On the other hand, the RZ-DPSK and RZ-DQPSK illustrate a much more tolerant range of [-5,9] dBm for the SMF input power and [-4,8] dBm for the DCF, for both formats.

Fig. 6, 7 also show two fundamental results. First, the RZ-DPSK and RZ-DQPSK modulation formats can easily bridge the 1,000…1,500 km distance range with a numerically estimated BER $\leq 10^{-9}$. This first conclusion is very important if we remember that one of the requirements for such systems, in many European size countries, is to always be able to use protection paths, likely to be in this distance range. Second, the considered ASK formats are more suited for metro and short haul applications, due to their low input power tolerance for higher distances applications. Finally, Fig. 8 shows that, in addition to a very good dispersion tolerance, the 10×10 Gbit/s NRZ DWDM scheme has a good system reach of 1,600 km. The main disadvantages remain its very low spectral efficiency as shown below and its significant operational complexity from an operator's point of view.

.

Table 1 summarizes the obtained results in terms of system reach and spectral efficiency of all the considered ASK and PSK formats. Additionally, this chart presents the system reach, also for a targeted 10^{-9} BER, of an alternating dispersion compensation scheme which is known for its ability to extend link lengths [8,9]. The RZ-DQPSK

format, providing the longest system reach, was also investigated for a non-zero dispersion shifted fiber type (NZDF). This lead to another significant reach extension of 11 more spans to a total of 2,800 km as shown in Fig. 9 and Table 1.

Table 1. System reach in multiples of 80-km SMF spans for a 10^{-9} BER target. $Reach_{ADC}$ is the alternating dispersion compensation configuration reach. SpecEff refers to the spectral efficiency of the considered format.

Format	Reach [spans]	Reach [km]	$Reach_{ADC}$ [km]	$Improvement_{ADC}$ [spans]	SpecEff [bit/s/Hz]
RZ-DQPSK (NZDF)	**35**	**2,800**	**---**	**---**	**0.94**
RZ-DQPSK	**24**	**1,920**	**1,440**	**-6**	**0.94**
RZ-DPSK	**20**	**1,600**	**1,840**	**+3**	**0.54**
10×10 Gbit/s NRZ	**20**	**1,600**	**---**	**---**	**0.22**
DQPSK	**17**	**1,360**	**1,280**	**-1**	**1.43**
DPSK	**15**	**1,200**	**1,440**	**+3**	**0.71**
RZ 0.5	**11**	**880**	**960**	**+1**	**0.54**
CS-RZ 0.66	**11**	**880**	**880**	**0**	**0.56**
NRZ	**7**	**560**	**640**	**+1**	**0.70**
NRZ-VSB	**5**	**400**	**---**	**---**	**0.69**
ODB	**3**	**240**	**320**	**+1**	**1.25**

Table 1 illustrates the two categories that appear when considering system reach. Indeed, the entire PSK formats are found to have a minimum reach of 1,200km with a maximum of 2,800 km for the RZ-DQPSK format using the NZDF fiber type. On the other hand the ASK schemes range between 240 km to 880 km for the RZ format with

0.5 duty cycle. Furthermore, despite all its advantages mentioned previously, the 10×10 Gbit/s NRZ (DWDM) scheme has the worst spectral efficiency with 0.22 bit/s/Hz, making its use comparably inefficient for 100 Gbit/s carrier Ethernet.

Finally, in these simulations, (N)RZ-DPSK formats are found to have less reach than (N)RZ-DQPSK despite a higher robustness to nonlinearities. This result might find an explanation in the fact that the total input power into the DCF was kept relatively small to prevent long simulation times due to the DCF high nonlinear coefficient γ_{DCF} = 5.27 1/W/km. Indeed the DCF role in our case was just to compensate exactly for the accumulated dispersion, the nonlinearities coming mainly from the propagation in the SMF over several spans. Moreover, the system reach was considered for a 10^{-9} BER requirement based on an extrapolation that has its intrinsic error for such low BERs; this can affect the accuracy of the found reach values as well. Nonetheless, for an alternated dispersion compensation scheme, the (N)RZ-DPSK reach normally outperforms the (N)RZ-DQPSK one as shown in column 4 of Table 1.

1.5 Conclusion

Performance of 100 Gbit/s serial transmission was investigated by means of numerical simulations. While the ODB format was found to be the most tolerant to dispersion (for low enough input powers), making it suitable for short haul 10→40Gbit/s upgrade, the RZ-DQPSK format, with 1,920 km reach and 0.92 bit/s/Hz spectral efficiency, outperforms all other schemes including the 10×10 Gbit/s NRZ DWDM inverse multiplexing that suffers from a very low spectral efficiency. A higher spectral efficiency can also be added to this format using polarization [10] or new subcarrier multiplexing techniques [11].

REFERENCES

1. G. Lehmann, R.H. Derksen, C. Schubert, M. Winter, "100 Gigabit Ethernet Transmission - Physical Layer Issues," in: Optical Fiber Communication Conference, Optical Society of America, 2007. p. OThD5.

2. E. Lach, K. Schuh, B. Junginger, G. Veith, J. Lutz, M. Möller, "Challenges for 100 Gbit/s ETDM Transmission and Implementation," in: Optical Fiber Communication Conference, Optical Society of America, 2007. p. OWE1.

3. P. A. Humblet and M. Azizoglu, "On the bit error rate of lightwave systems with optical amplifiers," J. Lightwave Technol. 9 (1991) 1576.

4. B. Slater, S Boscolo, T Broderick, S.K. Turitsyn, R. Freund, L. Molle, C. Caspar, J. Schwartz, and S. Barnes, "Performance analysis of 20Gb/s RZ-DPSK non-slope matched transoceanic submarine links," Opt. Express 15 (2007) 10999.

5. N. S. Bergano, F. W. Kerfoot, and C. R. Davidson, "Margin measuremnets in optical amplifier systems," IEEE Photon. Technol. Lett. 5 (1993) 304.

6. G. Bosco and P. Poggiolini, "On the Q factor inaccuracy in the performance analysis of optical direct-detection DPSK systems," IEEE Photonic. Technol. Lett. 16 (2004) 665.

7. E.G. Shapiro, M.P. Fedoruk, S.K Turitsyn, “Direct modelling of error statistics at 40 Gbit/s rate in SMF/DCF link with strong bit overlapping,” Electron. Lett. 40 (2004) 1436.

8. D. Breuer, F. Küppers, A. Mattheus, E.G. Shapiro, I. Gabitov, S.K. Turitsyn, “Symmetrical dispersion compensation for standard monomode-fiber-based communication systems with large amplifier spacing,” Opt. Lett. 22 (1997) 982.

9. D. Breuer, K. Jürgensen, F. Küppers, A. Mattheus, I. Gabitov, S.K. Turitsyn, “Optimal schemes for dispersion compensation of standard monomode fiber based links,” Opt. Commun,” 140 (1997) 15.

10. H. Wernz, S. Herbst, S. Bayer, H. Griesser, E. Martins, C. Fürst, B. Koch, R. Noe, A. Ehrhardt, L. Schürer, S. Vorbeck, M. Schneiders, D. Breuer, R.-P. Braun, “Nonlinear behaviour of 112 Gb/s polarisation-multiplexed RZ-DQPSK with direct detection in a 630 km field trial,” in Proc. of 35th *European Conference on Optical Communication (ECOC 2009), Vienna, Austria, Tu 3.4-3 (2009)*.

11. S. Xiao and A.M Weiner, “4-user, ~ 3GHz-spaced Sub-Carrier Multiplexing (SCM) using optical direct-detection via hyperfine WDM,” IEEE Photonic. Technol. Lett. 17 (2005) 2218.

CHAPTER 2

SERIAL 100 GBIT/S PM-RZ-DQPSK TRANSMISSION IN THE PRESENCE OF PERTURBATIONS FROM LOWER DATA RATE NEIGHBORING CHANNELS

2.1 Introduction

The dramatic increase in bandwidth demand driven by the rapidly expanding internet traffic urges to a necessary upgrade of the existing optical, regional and long haul transport networks. Advanced modulation formats, higher bit rates and increased spectral efficiency are indeed all required to meet this new challenging market demand. The 100 Gbit/s PM-RZ-DQPSK format (Polarization Multiplexed Return to Zero Differential Quadrature Phase Shift Keying) is already considered as one of the best candidates and is being more and more implemented in existing long haul networks. Because a total replacement of the existing optical transponders is practically impossible and financially out of cost; an objective and thorough study of the influence of existing channels on the new upgrade has to be realized. This chapter investigates the influence of existing 10 Gbit/s NRZ, 40 Gbit/s DPSK channels on a 100 Gbit/s PM-RZ-DQPSK central channel.

Because the main limitations at such bitrates are due to intra and inter-channel nonlinear effects, polarization impairments are not considered. The 100Gbit/s PM-RZ-DQPSK is consequently simulated by a 50 Gbit/s RZ-DQPSK that accounts for the 25 GBaud/s physical signal. Numerical Simulations are carried out for different numbers of neighboring channels while the power per channel is varied. BER estimates are also

obtained using the tail extrapolation technique that is presented and explained in this paper. Finally, a discussion of the observed trends and the accuracy of the results are considered at the end.

2.2 SIMULATION SETUP

The simulation setup is presented in Fig. 1. In this case, two 10Gbit/s NRZ neighboring channels are illustrated with a central 50 Gbit/s RZ-DQPSK channel (centered at 193.1 THz) that emulates the behavior of the 100 Gbit/s PM-RZ-DQPSK format without considering polarization effects, as explained before. For an optimum spectral efficiency, the channel spacing is set to 50 GHz for the 10Gbit/s NRZ and 40 Gbit/s DQPSK neighbors formats and to 100GHz for 40 Gbit/s DPSK format.

Each Channel is amplified with a separate EDFA that has a 5dB noise Figure. The EDFA gain is varied so that a constant power per channel between -4 to 6dBm is generated. The neighboring and central channels are then coupled using a theoretical coupler that can take N inputs and multiplex them into one single fiber. The combined signal is then passed through another EDFA that compensate for the coupler losses before entering the 10×80 km spans of standard single mode fiber (SSMF). Each span is constituted of an 80 km SSMF followed by an EDFA that adjusts the total power at the input of a dispersion compensated fiber (DCF) of 16km length. The DCF compensates exactly for the accumulated dispersion inside the SSMF. The output of the DCF is then connected to a new EDFA which task is to amplify the signal before entering again into the loop. After passing the 10 spans, the signal is filtered using a 50GHz bandwidth, 10^{th}

order Gaussian filter that selects only the central RZ-DQPSK channel. The filtered signal is finally demodulated and the in-phase (I) and quadrature (Q) generated signals are analyzed using a fully numerical bit error rate tester (BERT). The detailed parameters of the SSMF and DCF are presented below Fig. 1.

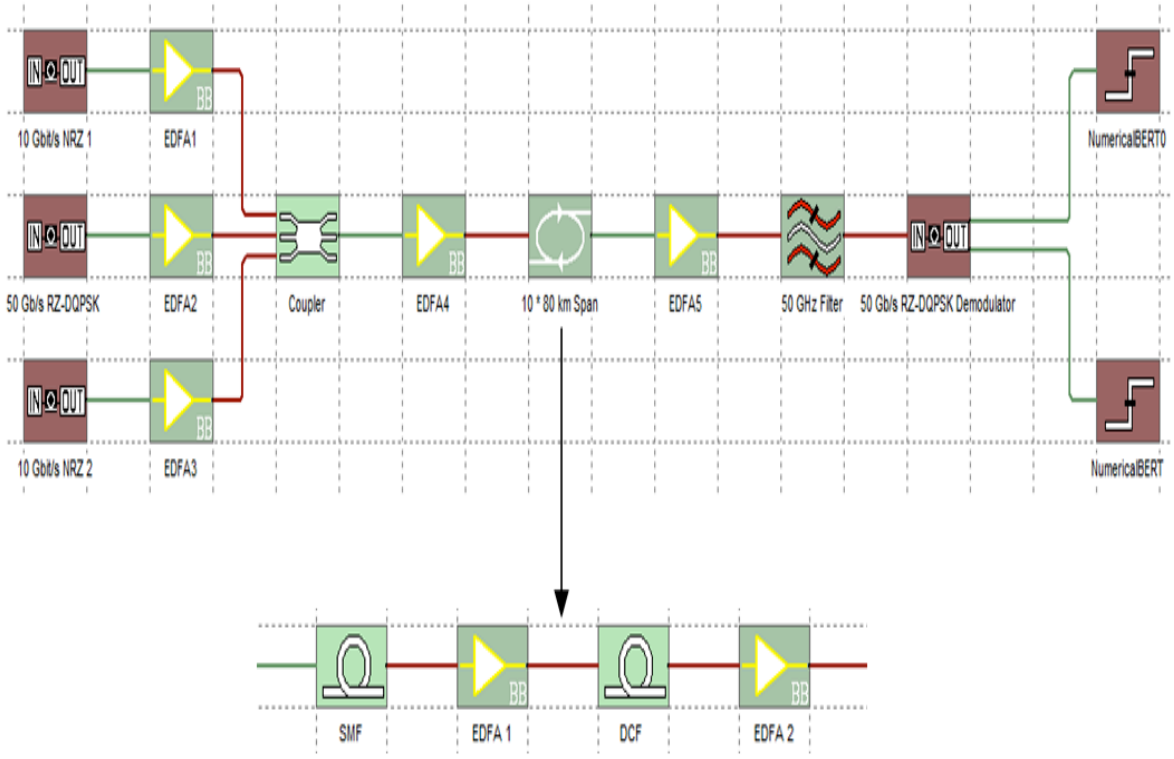

Fig. 1. Simulation setup illustrating a central 50Gbit/s RZ-DQPSK central channel with two neighboring 10 Gbit/s NRZ channels.

α_{SMF} = 0.2 dB/km, D_{SMF} = 16 ps/nm/km, ΔD_{SMF} = 0.09 ps/nm^2/km, γ_{SMF} = 1.317 /W/km
α_{DCF} = 0.5 dB/km, D_{SCF} = -80 ps/nm/km, ΔD_{DCF} = -0.15 ps/nm^2/km, γ_{DCF} = 5.28 /W/km
(α: attenuation, D: chromatic dispersion, ΔD: dispersion slope, γ: nonlinear coefficient).

2.3 TAIL EXTRAPOLATION

When realistic BER estimates are needed, the simulation procedure becomes critical for both the feasability and the accuracy of the results. Indeed, a direct bit error count method can be very time consuming when low BER are expected. For instance, if a BER of 10^{-9} is targeted with a a good precision, the number of simulted bits has to be at least two order of magnitude larger than 10^{9}, in other words, 10^{11} bits are needed. This requirement, combined with a large number of channels each with a possible high input power (9 channels each at 6dBm average power for the extreme case), a total length of 960 km of fiber (total SMF and DCF) can mean months and months of simulation. On the other hand, It's now widely accepted that a simple BER estimation from the Q-facor, assuming a Gaussian noise statistics, can lead to incorrect results for PSK formats.

Consequently, a tradeoff has to be found in order to obtain reliable results in a reasonable time. The solution proposed in this paper is the tail extrapolation of the marks' (logical ones) and spaces' (logical zeros) probability density functions (PDF). This method estimates very low BERs from fewer simulated bits, typically 10^{4}, 10^{5} bits. A low BER corresponds to a low likelihood for an error to occur; this information being contained in the tail of the probability density, our approach is to deduce the tail evolution from the center of the probability density that corresponds to high error occurencies. To realize this extrapolation, we assume that the marks and spaces PDFs have a generalized exponential shape described by (1)

$$p_x(x) = \frac{\delta}{2\sqrt{2}\Gamma(\frac{1}{\delta})\varepsilon} \exp\left[-\left|\frac{x-m_x}{\sqrt{2}\varepsilon}\right|^{\delta}\right] \quad (1)$$

Where Γ is the gamma function and ε, δ are fitting parameters for a least square fit. The BER is then given by (2)

$$BER = \int_S^{\infty} p_x(x)dx \approx \exp\left[-\left(\frac{S-m_x}{\sqrt{2}\varepsilon}\right)^{\delta}\right] \quad (2)$$

S being the decision threshold that determines whether the bit is a logical 1 or 0. In order to find the lowest BER estimate, we sweep S over the actual bit error counts range. For every position, the BER is calculated by counting the number of errors, then, the optimum one is extrapolated using Eq. 1 to deduce first the best PDF fit and Eq. 2 to solve for the minimum BER value. One can easily see here that the minimum accessible BER before extrapolation for 10^4 bits is 10^{-4} as shown in Fig. 2 (b).

Fig. 2 (a) presents the balanced detected eye diagram of the central channel for two 10Gbit/s NRZ neighbors after 5 spans. Fig. 2 (b) shows the log(BER) evolution when the threshold is swept over the eye range. After extrapolation the optimum BER corresponds to the intersection of the gray and the green curves.

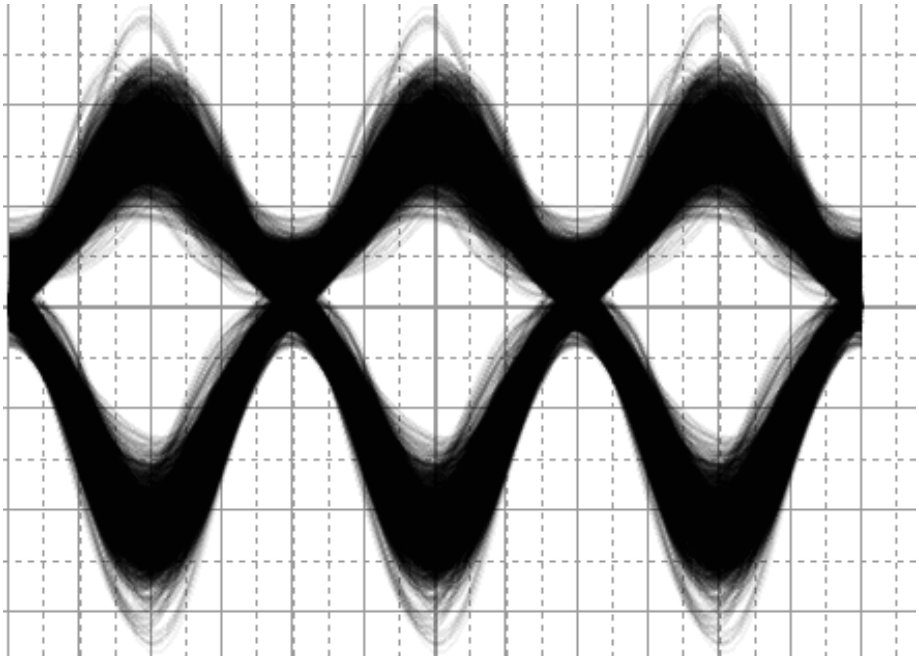

(a)

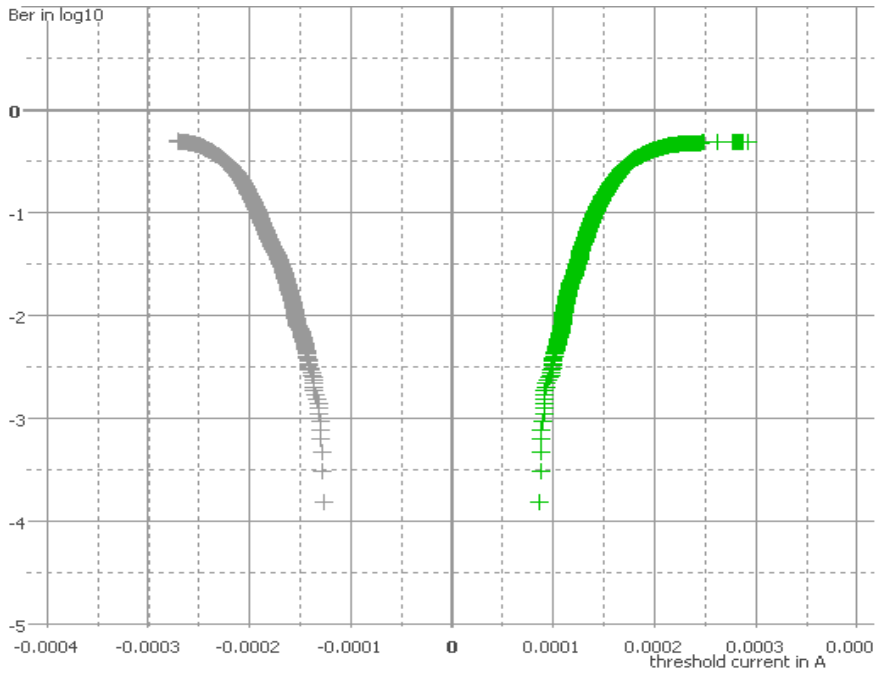

(b)

Fig. 2 (a) Eye diagram after balanced detection at the receiver side, (b) log(BER) evolution for different threshold values

2.4 SIMULATION RESULTS

The simulations are carried out for the following neighboring channels: 1, 2, 4, 6 and 8 ×10Gbit/s NRZ neighbors with 50 GHz channel spacing, see dashed curves in Fig 3. (a, b). We also present BER estimates of the central probe for 1, 2, and 4 ×40Gbit/s DPSK neighboring channels with 100GHz channel spacing, see continuous lines in Fig. 3 (a).

Finally, for clarity and simplicity reasons Fig. 3 (b) shows the results for 1, 2, 4, 6 and 8 ×40Gbit/s DQPSK neighbors with 50GHz channel spacing along with those of NRZ taken as a reference.

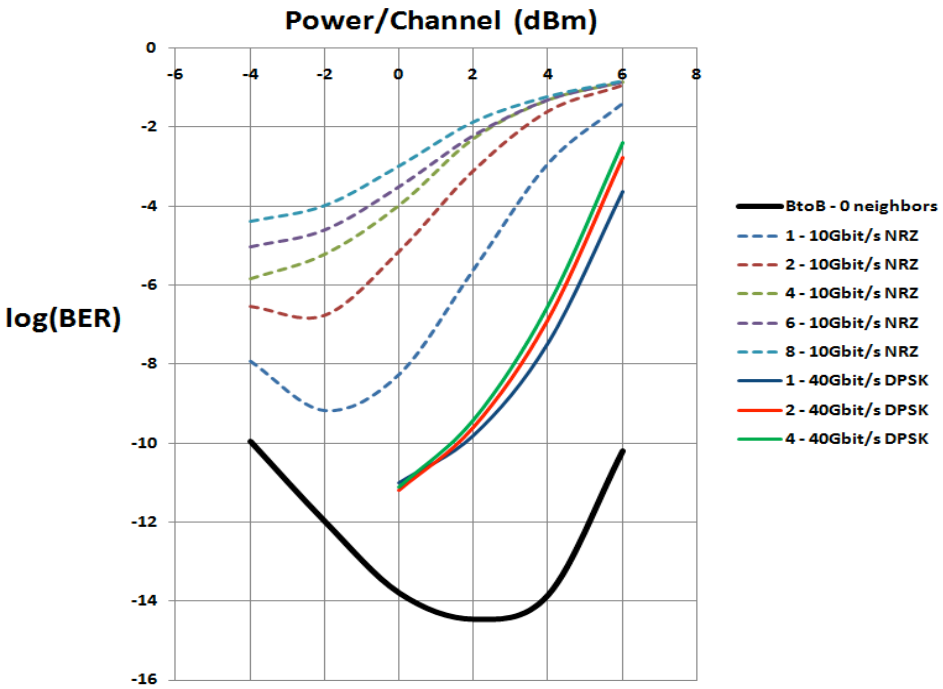

(a)

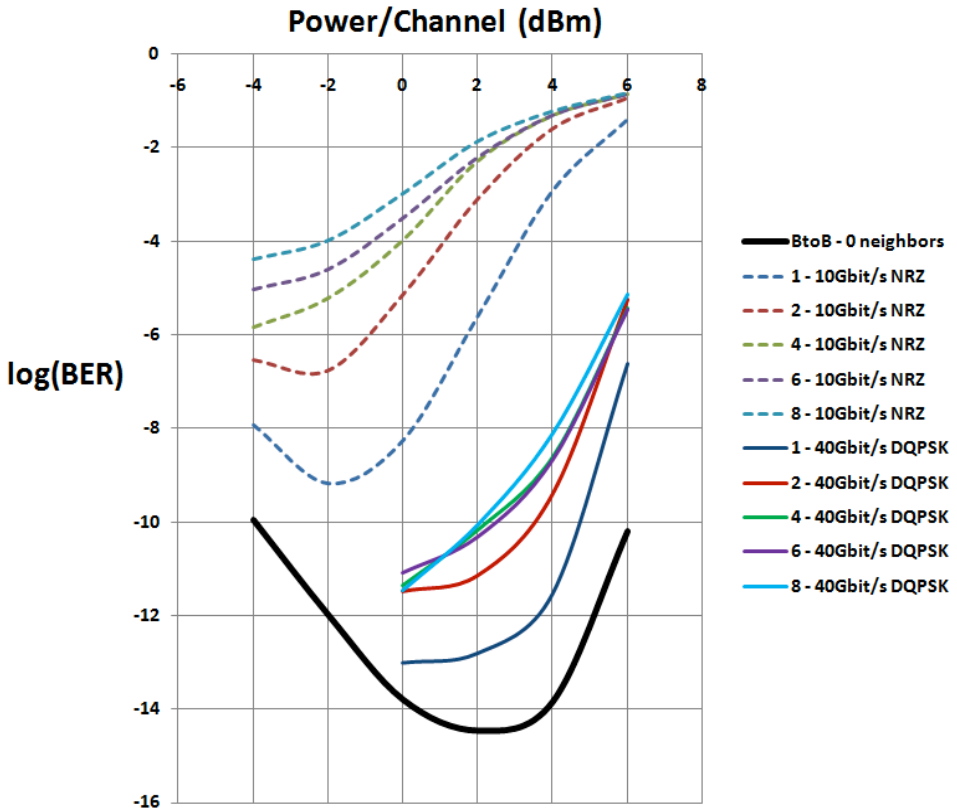

(b)

Fig. 3. BER evolution of the 100 Gbit/s PM-RZ-DQPSK equivalent probe for an increased power per channel and for different numbers of (a) 10Gbit/s NRZ (50 GHz channel spacing) and 40 Gbit/s DPSK (100GHz channel spacing) neighbors, (b) 10Gbit/s NRZ and 40 Gbit/s DQPSK (both 50 GHz channel spacing) neighbors

2.5 DISCUSSION

The black curve in Fig. 3 (a, b) represents the system in its back to back configuration. We see that in this case the optimum input power of the probe is around 2 dBm with a BER of ~ 10^{-14}. When one 10 Gbit/s NRZ neighbor is added with 50 GHz channel spacing, the BER of the central channel increases very rapidly and sees its minimum shift towards less power per channel -4 dBm corresponding to a minimum BER of ~ 10^{-9}. For 2, 4, 6 and 8 ×10 Gbit/s NRZ neighboring channels the BER increases less rapidly (the

curves get gradually stacked together) and the minimum continues to shift towards less input power per channel. In the case of the 1, 2 and 4×40 Gbit/s DPSK neighbors, we see in Fig. 3 (a) a sharp decrease in the BER of the probe but all the curves are superimposed and show a better behavior than the NRZ case. A minimum BER of ~ 10^{-11} is reached by the probe for a power per channel between [-2, 0] dBm. Note that in this case, we had to increase the channel spacing to 100 GHz to avoid too much spectral overlapping that impairs the central channel very quickly. Fig. 3 (b) shows on the other hand the BER evolution of the probe when 1, 2, 4 6 and 8 ×40 Gbit/s DQPSK neighboring channels are added. In this case the probe presents the best results with a minimum BER of ~ 10^{-12} for 0 dBm input power per channel. When the power per channel is increased the BER increases more gradually meaning that probe is less affected by the nonlinearities. Moreover, the central probe has the approximately same response to 2, 4, 6 or 8 ×40 Gbit/s DQPSK neighbors (the BER curves form a pile).

In order to explain these trends, we need to remember that cross phase modulation (XPM) is a main limitation for multiplexed PSK format. Indeed, this nonlinear impairment takes place when the intensity modulation of one channel modulates the phase of a neighboring one. The presented results show clearly that the central probe is the most affected by XPM when the 10 Gbit/s NRZ channels are added. This first conclusion is coherent considered that NRZ format is an intensity modulated format (IM) that can be source of XPM on the central probe especially for a high input power per channel. Furthermore, it's interesting to notice that for one 10 Gbit/s NRZ neighbor a

BER of 10^{-9} for the central channel can be achieved. If more NRZ neighbors are desired, forward error correction (FEC) has to be considered.

For 40 Gbit/s DPSK and DQPSK neighboring channel, XPM is less critical. In this case, the central probe is mainly affected by four wave mixing (FWM) that arises as soon as more that one channel is added to the central probe. The piles that the BER curves form in Fig. 3 (a, b) suggest that FWM is mainly due to the two very first neighbors at 193.2 and 193 THz for DPSK and 193.15 and 193.05 THz for DQPSK neighbors.

2.6 CONCLUSION

Effects of neighboring 10 Gbit/s NRZ, 40 Gbit/s DPSK and 40 Gbit/s DQPSK channels on a central 100 Gbit/s PM-RZ-DQPSK probe were investigated. Although polarization effects were not considered, the results show that NRZ format through XPM has the most deleterious effect on the probe. DPSK and DQPSK formats are more critical when the number of channels and the power per channel are increased. FWM is the main limitation in this case.

REFERENCES

1. M.C. Jeruchim, P. Balaban, K.S. Shanmugan, "Simulation of Communication Systems," *Plenum Press*, New York / London (1994).

2. M.C. Jeruchim "Techniques for Estimating the Bit Error Rate in the Simulation of Digital Communication Systems," *IEEE J. Select. Areas Commun*., vol. 2, no. 1, pp. 153-170 (1984).

3. H. Wernz, S. Herbst, S. Bayer, H. Griesser, E. Martins, C. Fürst, B. Koch, R. Noe, A. Ehrhardt, L. Schürer, S. Vorbeck, M. Schneiders, D. Breuer, R.-P. Braun, "Nonlinear Behaviour of 112Gb/s Polarization Multiplexed RZ-DQPSK with Direct Detection in a 630 km Field Trial," in Proc. of 35th *European Conference on Optical Communication (ECOC 2009). Vienna, Austria, Mo 3.4.3 (2009).*

4. M. N. Islam *et al.*"Cross-phase modulation in optical fibers," Opt. Lett. 12 (8), 625 (1987).

5. G. P. Agrawal, *Nonlinear Fiber Optics*, 4th edn., Academic Press, New York (2006).

6. C. W. Thiel, "Four-wave mixing and its applications," http://www.physics.montana.edu/students/thiel/docs/FWMixing.pdf

CHAPTER 3

ALL-OPTICAL PROCESSING OF RZ-DPSK SIGNALS USING COUNTER-PROPAGATING PULSES IN A SATURATED SOA

3.1 INTRODUCTION

All-optical signal processing has garnered much attention especially in applications with high data rates or where several wavelength division multiplexed (WDM) channels can be processed simultaneously. Examples of all-optical signal processing include optical regeneration [1], wavelength conversion [2], and clock recovery [3].

The semiconductor optical amplifier (SOA) is a suitable device for all-optical signal processing due to its high gain, nonlinear properties, and fast recovery time. All-optical signal processing techniques using SOAs include pulse amplitude equalization for clock recovery [4], wavelength conversion [5], regenerative amplification [6], and extinction ratio improvement [7].

In this chapter, the interaction of counter-propagating pulses in a saturated SOA provides these optical signal processing functionalities. As shown in Fig. 1 (a), a return-to-zero differential phase-shift-keyed (RZ-DPSK) signal is input into a delay interferometer (DI) with one-bit delay which converts (or phase-demodulates) the RZ-DPSK signal into an amplitude-shift-keyed (ASK) signal. The amplitude modulated signals from the two outputs of the DI are logical opposites. These two signals then counter-propagate in the saturated SOA. During every bit slot, a strong pulse or mark, representing binary data, enters one side of the SOA, and a weak “pulse” or space, consisting of noise, enters the other side. This scheme has already been proven as the

central processing unit in a passive optical network (PON) extender [8] and a similar setup has been proposed as a method for phase regeneration of phase-noise-degraded RZ-DPSK signals [9].

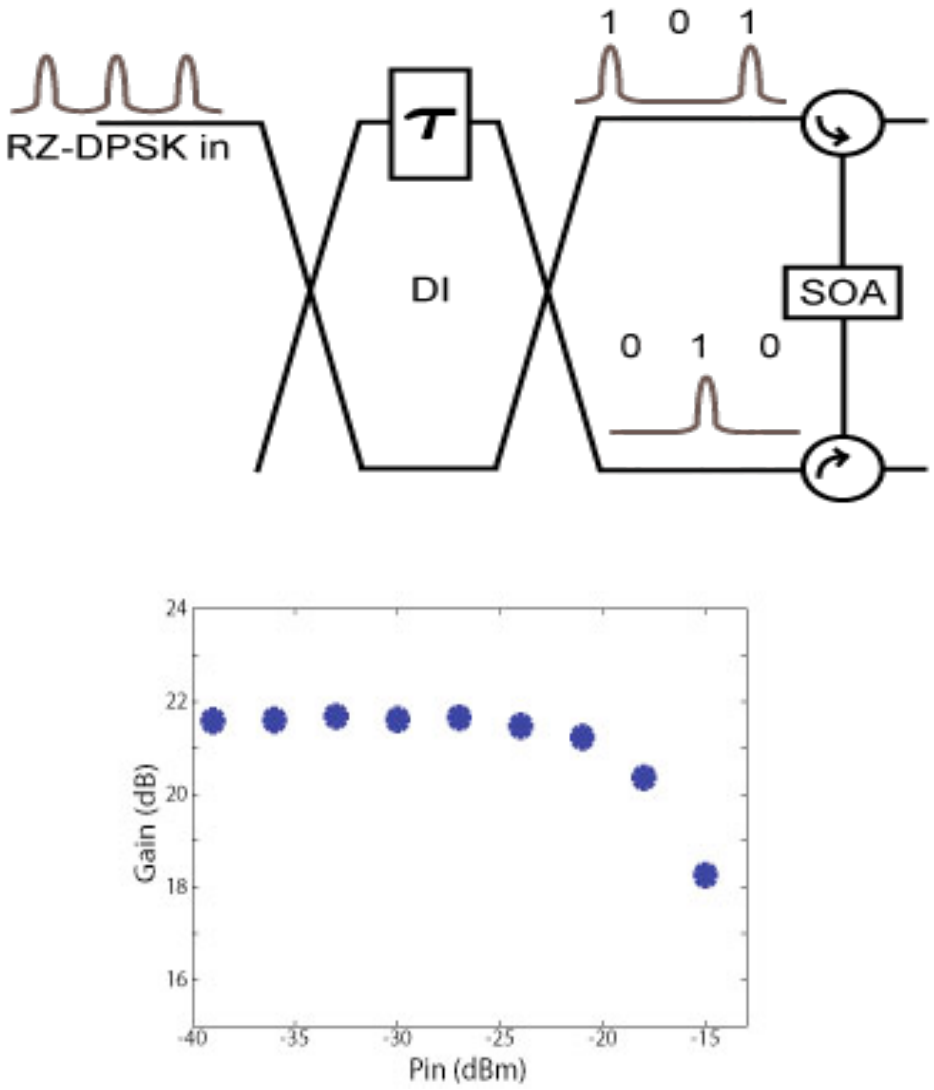

Fig. 1. (a) Schematic of counter-propagating pulses in a saturated SOA. An RZ-DPSK signal is phase demodulated by a one-bit delay interferometer and the logically opposite signals counter-propagate in the SOA. (b) Gain vs. input power for the SOA used in the experiment.

We demonstrate three novel methods of optical signal processing for received RZ-DPSK signals using this scheme: (a) Amplitude restoration after modulation format conversion from PSK to ASK, (b) photonic balancing, and (c) saturated asymmetric filtering both demonstrated by means of experimental BER measurements.

It is important to note that none of these three methods is intended to regenerate the initial RZ-DPSK signal in the sense of an in-line regenerator. In fact, self-phase modulation from the saturated SOA would ultimately counteract any achieved improvement when converting the demodulated signal back into the phase domain.

(a) The SOA in this counter-propagating pulses scheme provides Q-factor improvement of the demodulated signal through gain saturation and amplified spontaneous emission (ASE) modulation. For the first time we demonstrate how this optical signal processing technique can restore the amplitude of the demodulated signal leading to a 3.5 dB improvement in Q-factor.

(b) With photonic balancing the saturated SOA creates a differential signal and provides functionality analogous to electrical balanced detection. For the first time we give a thorough explanation of the theory behind photonic balancing and demonstrate that photonic balanced detection leads to a ~ 3 dB reduction in required optical signal to noise ratio (OSNR) over single-ended detection.

(c) Finally we demonstrate saturated asymmetric filtering which provides a method to remove in-band ASE noise from a signal before detection. These three

methods are demonstrated experimentally by analyzing eye diagrams and measuring BER at 10.7 Gb/s and 22.3 Gb/s.

3.2 EXPERIMENTAL SETUP

To demonstrate these concepts, the experimental setup shown in Fig. 2 was used. The optional components are shown in the dashed boxes. The signal generated with DFB lasers operating at 1550.0 nm and Mach-Zehnder modulators was either a carrier suppressed return to zero (CS-RZ) pulse stream with 22.3 GHz repetition rate and 67% duty cycle or a 10.7 Gb/s RZ-DPSK signal with 33% duty cycle modulated with a pseudo-random bit sequence (PRBS 2^{23}-1). Note that both signals have a pulse duration of 30 ps. The CS-RZ pulse train created with a 11.15 GHz clock signal was unmodulated and consisted of a periodic sequence of pulses with alternating phase of 0 or π. Either signal was intentionally combined with a broadband noise source (i.e., ASE noise) which had an optional 20 GHz optical bandpass filter. A variable optical attenuator controlled the noise power. The noisy signal was amplified by an erbium-doped fiber amplifier (EDFA). An optical spectrum analyzer (OSA) was used to measure the OSNR. An optional bandpass filter, a variable attenuator, and an optional SOA followed the EDFA. The signal was demodulated by a DI with free spectral range of either 10.7 GHz or 22.3 GHz. A sampling oscilloscope and a bit error rate tester (BERT) were used to measure the signal eye parameters and bit error ratio immediately after demodulation. The two arms of the DI were connected to either end of the SOA. A variable delay line ensured that the corresponding marks and spaces representing the same symbol arrived at the

SOA simultaneously and circulators separated the incoming signals from the outgoing signals. At the receiver a variable attenuator and a bandpass filter controlled the signal that was processed by the SOA and input into the sampling oscilloscope or the BERT.

In this work the SOA length was 1.6 mm, per the manufacturer, its linear gain 22 dB and the saturation output power 2 dBm for an applied bias current of 200 mA. The pulse length inside the SOA was 2.9 mm. If the pulse length was shorter than the SOA the presence of more than one pulse in the SOA changes the symmetry of the carriers' distribution and can degrade the system performance. This constraint defines practically the maximum applicable bit rate.

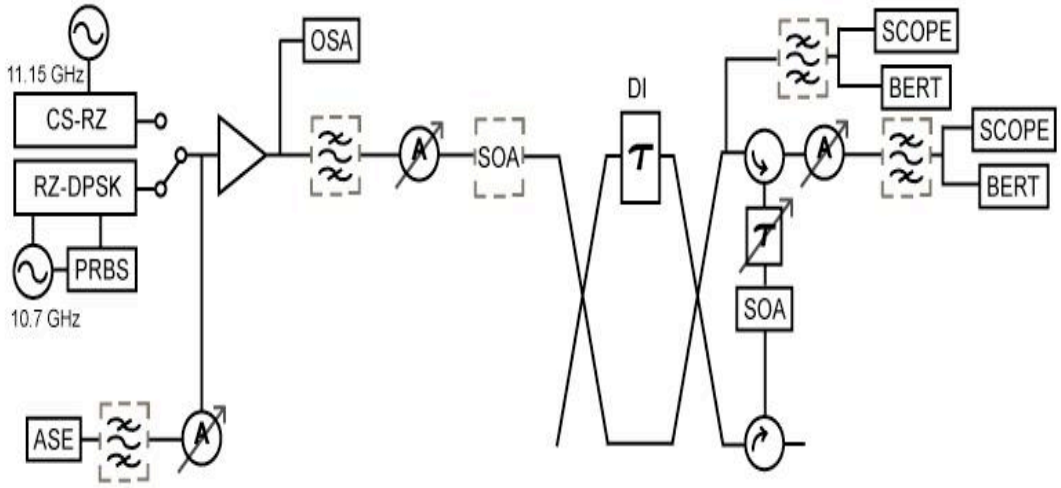

Fig. 2. Experimental setup for optical signal processing. The optional components are in the dashed boxes. An RZ-DPSK signal or a CS-RZ test signal are used. The four filters (20 GHz bandwidth) are only used with amplitude restoration, method (a), and saturated asymmetric filtering, method (c). The SOA before the DI is only used as a reference case for photonic balancing

3.3 AMPLITUDE RESTORATION AFTER FORMAT CONVERSION

3.3.1 Principle of Operation

Future transparent networks will provide all-optical methods to convert the modulation format of data signals. This conversion should be coupled with regeneration to ensure that impairments which affected the original signal do not degrade the converted signal. For example, a DI can provide modulation format conversion by demodulating an RZ-DPSK signal from a phase encoded signal to an amplitude encoded signal. The amplitude jitter of the demodulated signal is affected by both the amplitude fluctuations and the phase fluctuations of the original RZ-DPSK signal [10].

SOAs have been used previously for amplitude regeneration either with electro-absorbers [11] or in a Mach-Zehnder interferometer structure [12]. A single SOA in a conventional configuration cannot provide amplitude regeneration because noise is added to the spaces and the signal extinction ratio decreases [11]. The exception is the quantum dot SOA which has been demonstrated to provide amplitude regeneration [6], but these devices are far from commercialization.

With counter-propagating signals in an SOA, we demonstrate how a single commercially available SOA can be used for amplitude regeneration after a modulation format conversion. When operating in the nonlinear regime, an SOA can decrease the amplitude fluctuations of the marks, relative to the eye opening, by providing limiting amplification. When used in the counter-propagating configuration shown in Fig. 1, the marks ensure that the counter-propagating spaces obtain the same nonlinear gain as the marks. Also the marks limit the amount of ASE noise added to the spaces. This is due to the fact that the marks deplete the carriers available for spontaneous emission. This

maintains a high extinction ratio and prevents an excessive amount of added ASE noise. In this manner, the mark level fluctuations are decreased, and the space level fluctuations are not increased, relative to the eye opening. This improves significantly the Q-factor of the demodulated signal.

3.3.2 Experimental Results

To characterize the amplitude restoration capability, a CS-RZ test signal was used in the setup in Fig. 2 because it is physically the same as an RZ-DPSK signal with an alternating phase change between 0 and π. The advantage of using this signal is that after the DI all the marks are present on one arm and all the spaces are on the other, which allows to characterize separately the optical spectra of the marks and spaces. All four bandpass filters in Fig. 2 were used [13].

The standard deviations and means for the mark and space levels of the demodulated signal were measured directly with the sampling oscilloscope. For the spaces, the signal measured was ASE noise. The measured values are: $\sigma_{1,0}$, the standard deviation of the mark, space level, and μ, the difference between the means of the mark level and the space level. The values of σ_1 and σ_0 were normalized by μ. The corresponding Q-factor was $Q = \mu/(\sigma_1+\sigma_0)$.

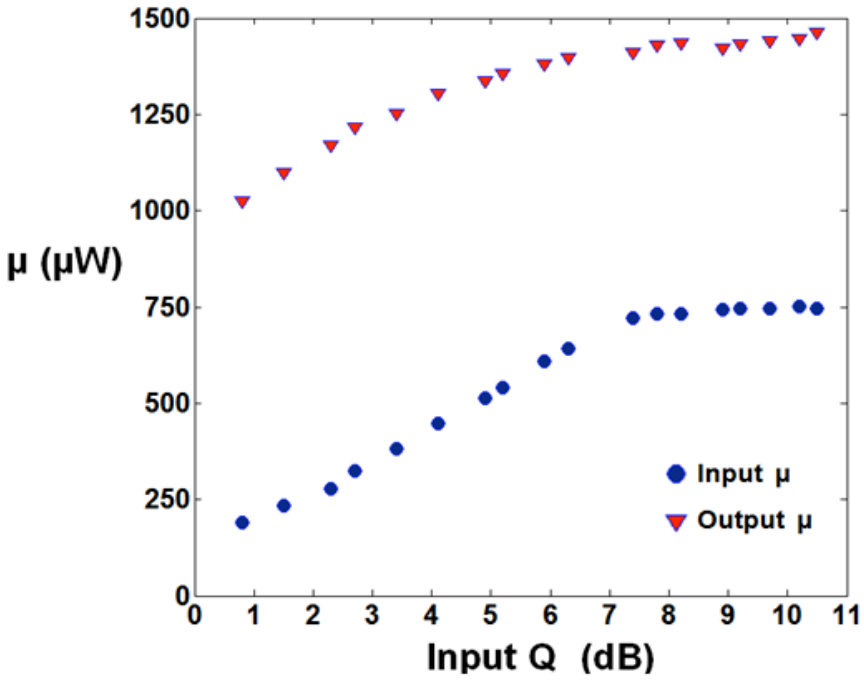
μ (μW)
Input Q (dB)
Input μ
Output μ

(a)

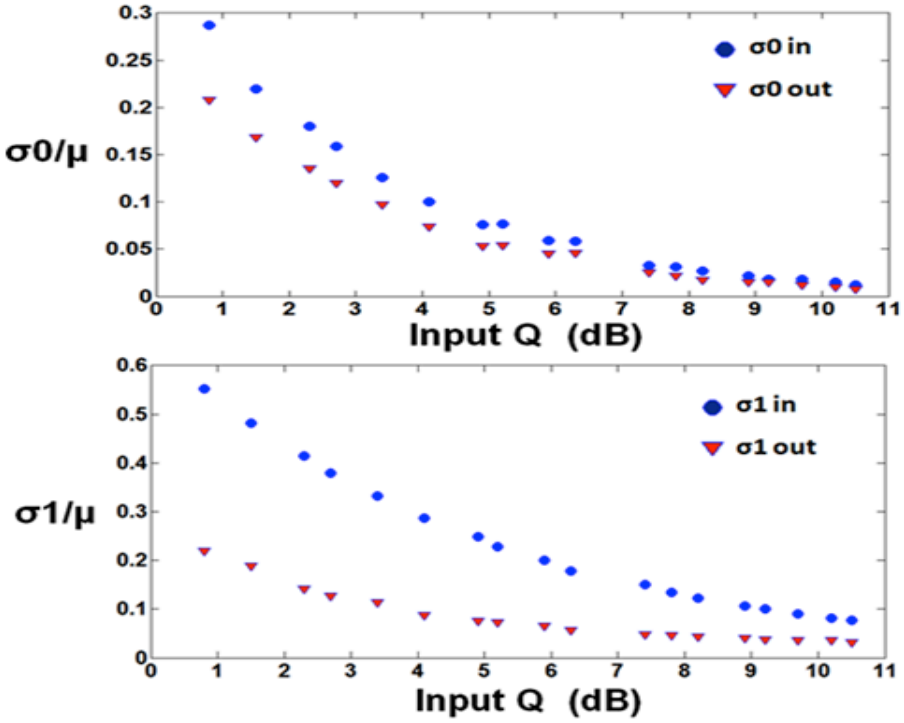
σ0/μ
σ0 in
σ0 out
σ1/μ
σ1 in
σ1 out
Input Q (dB)
Input Q (dB)

(b)

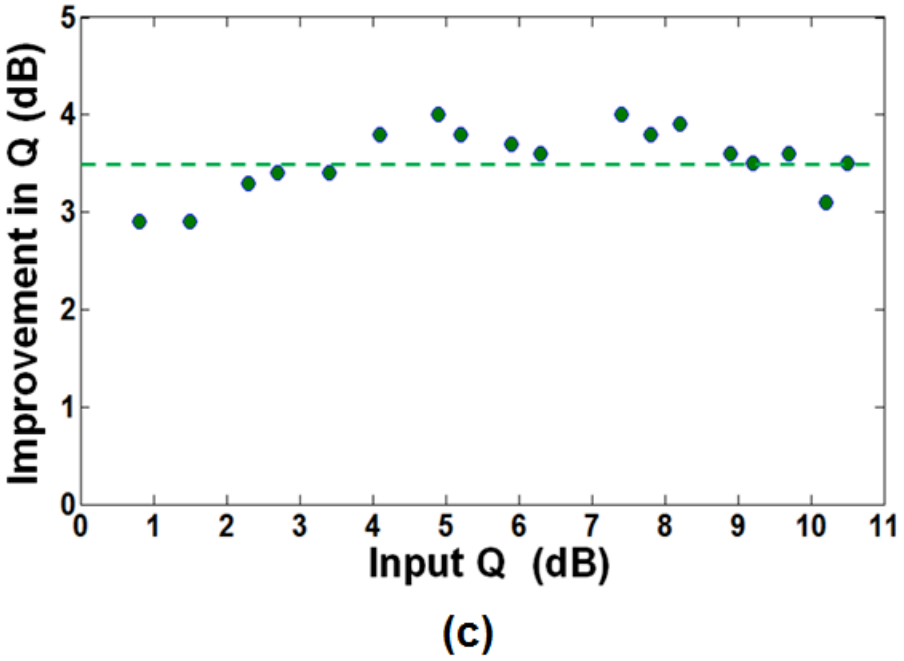

Fig. 3. (a) Mark and space separation, μ and (b) standard deviation of mark and space level $\sigma_{1,0}$, normalized by μ of the demodulated signal versus input Q. (c) Resulted improvement in Q-factor versus input Q.

Fig. 3(a) shows the measured value of μ at the input and at the output of the SOA as a function of input Q. The SOA increased the separation between the mark and space level for a wide range of input Q values. Fig. 3(b) shows the standard deviation of the mark and space levels (σ_1 and σ_0) normalized by μ at the input and output versus input Q-factor. After normalizing by μ, we see σ_0 is unchanged by the SOA, but σ_1 is decreased by the SOA. Fig. 3(c) shows that the simultaneous increase in μ and decrease in σ_1 without an increase in σ_0 lead to an improvement in Q of ~ 3.5 dB. Subsequent measurements using pseudo-random bit sequence (PRBS) RZ-DPSK signals yielded similar values. This is significantly higher than the 1.1 dB Q-factor improvement reported previously in a proof-of-concept demonstration [13].

3.4 PHOTONIC BALANCING

3.4.1 Principle of Operation

A new concept – introduced as photonic balancing [13] – carries out the same function as electrical balanced detection. When electrical balanced detection is used with RZ-DPSK signals, the required OSNR for a given BER is reduced by 2.7 dB [14] compared to single ended detection. This is due to the fact that balanced detection uses all the information from two symbols for each binary decision, doubling the signal power. The noise present in the two symbols is uncorrelated, and thus the noise power is not doubled [15]. Photonic balancing creates a differential signal optically which also uses the information from two symbols.

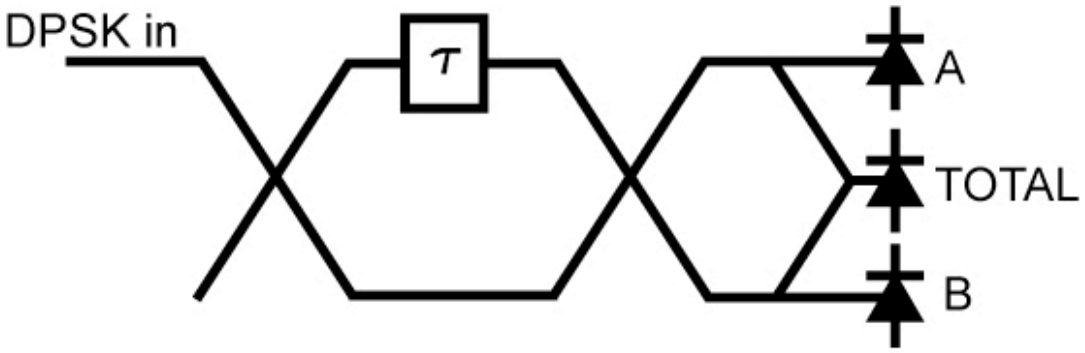

Fig. 4. General scheme for balanced detection with three photodiodes.

For explanation, we refer to Fig. 4 which is a general scheme for balanced detection. Fig. 4 shows a delay interferometer where each output arm is split into two by 3 dB

splitters. The uppermost arm goes to photodiode A, the lower one to photodiode B, and the middle two combine so that their total power is measured by photodiode TOTAL. Fig. 4 illustrates a principle without worrying about the practical realization, which would be more complicated than appears from drawing.

We can use any two of these photodiodes to achieve electrical balanced detection. The most common approach is to use photodiodes A and B by subtracting the electrical currents and comparing to 0. The decision equation is:

$$P_A - P_B \geq 0 \tag{1}$$

where P_A is the power from photodiode A, and P_B is from photodiode B. For example, if this difference is greater than 0, the symbol is interpreted as a binary 1 else it is interpreted as a binary 0.

Equivalently we can use photodiodes A and TOTAL. In this case the decision equation is:

$$P_A - \frac{P_{TOTAL}}{2} \geq 0 \tag{2}$$

where we compare the power from photodiode A to the total power from both arms of the delay interferometer. Since the total power is the sum of the power from A and B we show that (1) is equivalent to (3):

$$
\begin{aligned}
P_{TOTAL} &= P_A + P_B \\
P_A - \frac{P_{TOTAL}}{2} &= \frac{P_A - P_B}{2} \geq 0 \\
\Leftrightarrow P_A - P_B &\geq 0
\end{aligned}
\tag{3}
$$

For the second case, we need to measure P_{TOTAL} and thus the complexity is not reduced. If P_{TOTAL} is constant and known *a priori*, we only need to measure either P_A or P_B. We then compare the measured value to the constant P_{TOTAL}.

For a saturated SOA the total output power is nearly constant irrespective of input power. When used in the counter-propagating configuration the total output power is the sum of the output power of the mark and the output power of the space. The two symbols split the output power according to their relative strengths at the input. Whichever symbol has more power at the input will have more power at the output. By comparing the sampled output power from a single photodiode to the total output power which is known and constant, we can make a decision. This allows us to use the information present in two symbols while employing one photodiode. In this way, we can have the benefits of balanced detection, the 3 dB reduction in required OSNR, while using a single photodiode. While the SOA is not an ideal power limiter in the saturation regime, considering P_{TOTAL} as a constant is a reasonable approximation for our purposes.

Amplitude restoration, presented in section 3, and photonic balancing are a result of the same SOA attributes. The two processes have different applications and are characterized differently.

3.4.2 Experimental Results

To demonstrate photonic balancing, two SOA configurations were compared as shown in Fig. 2. A 10.7 Gb/s RZ-DPSK signal was used. Note that no bandpass filters included here.

For photonic balancing, counter-propagating pulses pass through the SOA with an average power into each side of the SOA of 10.6 dBm. As a reference, an SOA in conventional configuration was placed immediately in front of the DI and the signal was measured after the DI. The optimal average power into this SOA was -2 dBm which was the optimal power to minimize added phase noise to the signal. This optimized configuration is the best to compare to photonic balancing because the SOAs in both configurations provide a similar amount of gain. They also provide a similar amount of added ASE noise because a pulse enters the SOA and modulates the ASE noise during each bit slot for both cases.

Fig. 5 shows the bit error ratio (BER) versus input OSNR for both cases. The OSNR in this experiment is referenced to 0.1 nm noise bandwidth. For photonic balancing (PB), the required OSNR is ~ 3 dB less than for the reference case. This improvement is the same that would be provided if electrical balanced detection were used. Photonic balancing provides the same reduction in OSNR as electrical balanced detection.

When compared to a reference signal without an SOA, photonic balancing yields only a 1 dB reduction in OSNR. The improvement is less than balanced detection because the SOA used in photonic balancing adds some ASE noise to the signal.

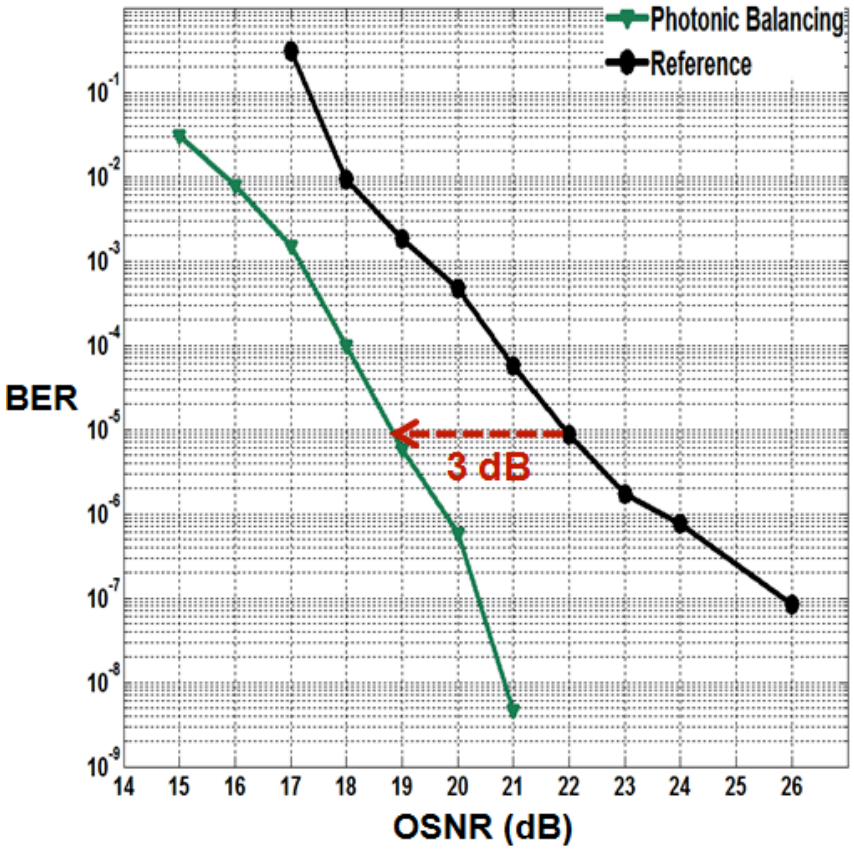

Fig. 5. BER versus OSNR for photonic balancing and reference signal. The reference signal was amplified by an SOA before demodulation. The OSNR values were referenced to 0.1 nm noise bandwidth.

3.5 SATURATED ASYMMETRIC FILTERING

3.5.1 Principle of Operation

With saturated asymmetric filtering, the highly saturated SOA generates an asymmetric spectrum. A filter detuned from the carrier frequency can take advantage of this induced asymmetry and filter out a significant portion of the in-band ASE noise [16].

As the marks traverse the SOA, they experience self-phase modulation (SPM). In addition to spectral broadening, the pulse is chirped such that lower frequencies are present in leading edge of the pulse and higher frequencies are in the trailing edge. The higher frequencies in the trailing edge experience less gain due to gain saturation than the lower frequencies in the leading edge. The spaces, which consist of noise, experience the same index modulation (red-shift) but are spectrally less broadened. A filter detuned from the original carrier frequency will pass the signal present in the marks while filtering out the in-band noise in the spaces. Since the saturated asymmetric filtering shifts the signal power towards one side of the spectrum, this new scheme can be considered as an enhanced version of the regenerative process proposed in [17].

3.5.2 Experimental Results

In order to illustrate this spectral power shift, a CS-RZ test signal was used according to the set-up shown in Fig. 2 such that after demodulation a sequence of marks was in one arm and a sequence of spaces in the other. The optical spectrum without any filtering is shown in Fig. 6. The vertical dashed line in Fig. 6 represents the original carrier frequency. The marks' spectrum is asymmetric with respect to the carrier frequency: more power is present in the red-shifted wavelengths than in the blue-sifted ones. Since the spaces are coincident with the marks at the SOA, they experience the same index

modulation; their spectrum is therefore asymmetric but less broadened because of their relatively low power.

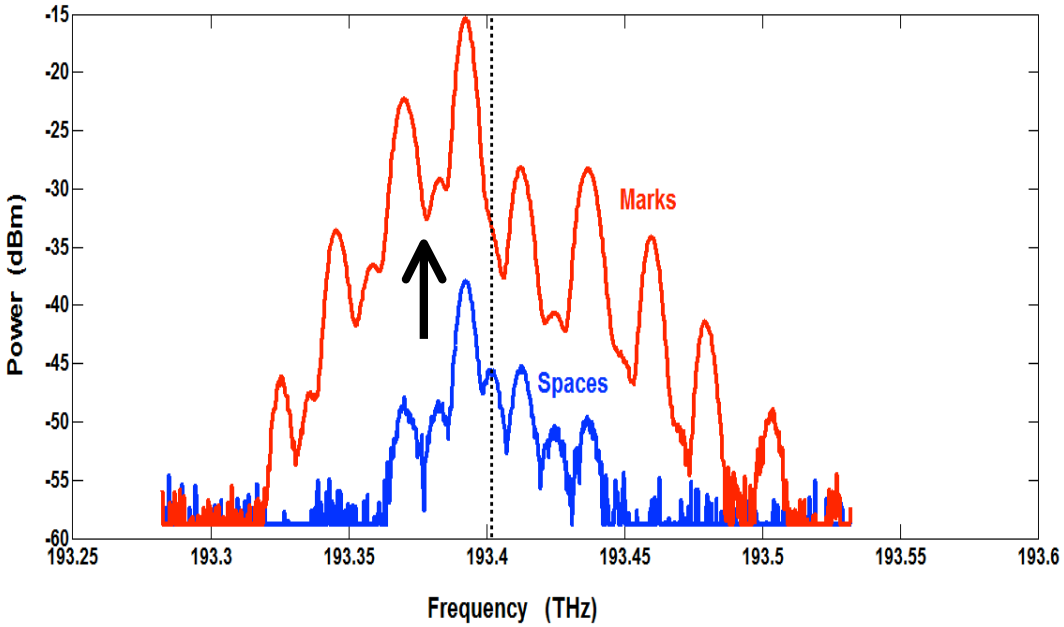

Fig. 6. Optical spectra of the marks (red) and spaces (blue) after counter-propagating in the highly saturated SOA.

Finally, the effect of saturated asymmetric filtering on the receiver performance was measured. As seen in Fig. 2, a 10.7 Gb/s RZ-DPSK signal was used and all four bandpass filters in Fig. 2 were present. The average power into the SOA was 18.5 dBm. The Gaussian-shaped bandpass filter of 20 GHz bandwidth connected directly after the SOA was detuned by Δf = 16.2 GHz from the carrier frequency, giving the optimum result. Fig. 7 shows BER versus the optical power P_{in} into the receiver for saturated asymmetric filtering for various filter shifts and the reference signal taken after the DI. As seen in Fig. 8, saturated asymmetric filtering improves the receiver sensitivity by 2.7 dB when

compared to the reference for a BER target $\leq 7\times10^{-8}$. This improvement is due to the fact that the in-band noise present in the spaces was filtered out by this scheme.

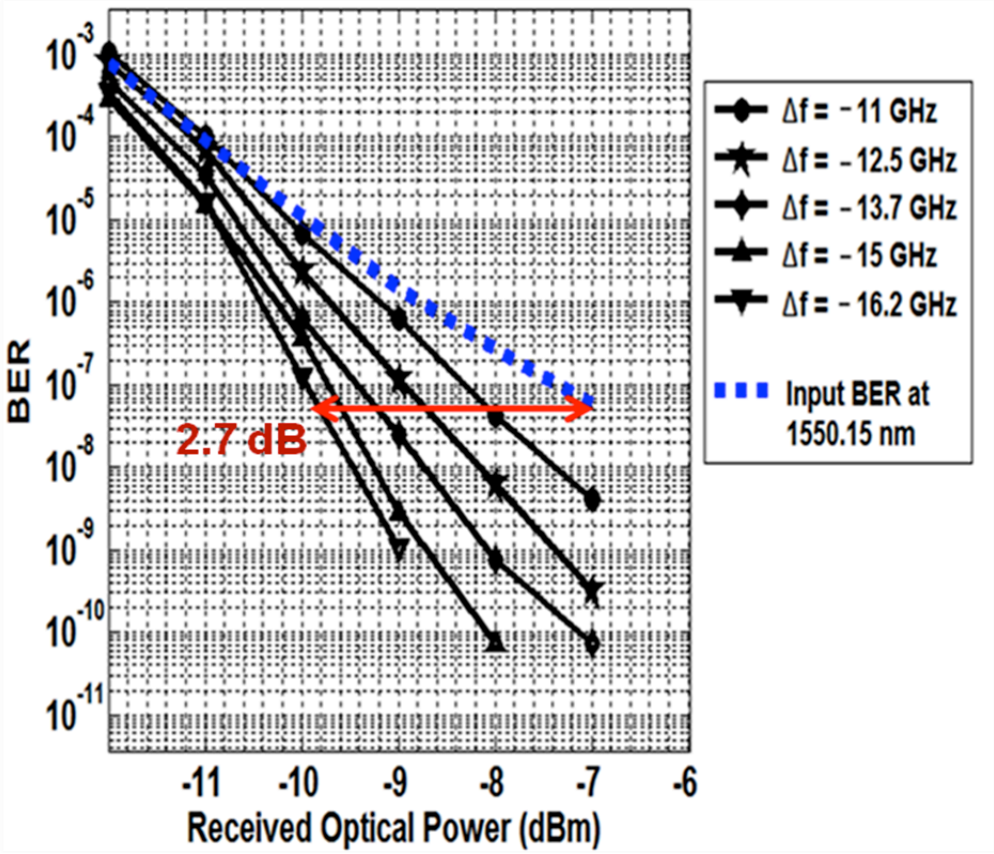

Fig. 7. BER versus P_{in} for saturated asymmetric filtering. The reference signal was taken after the delay interferometer. Filter bandwidth was 20 GHz.

3.6 Conclusion

We demonstrated Q-factor improvement after modulation format conversion, photonic balancing, and saturated asymmetric filtering using counter-propagating pulses in a saturated SOA. For the first time, we demonstrate a 3.5 dB improvement in Q-factor of the amplitude regenerated signal. For the first time, we demonstrate that photonic balanced detection leads to a ~ 3 dB reduction in required optical signal to noise ratio (OSNR) over single-ended detection. Finally, we demonstrate saturated asymmetric filtering which provides a method to remove in-band ASE noise from a signal before detection and leads to a 2.7 dB improvement in receiver sensitivity.

REFERENCES

1. Slavik, R. *et al.* "All-optical phase and amplitude regenerator for next-generation telecommunications systms," *Nature Photon.* **4,** 690–695 (2010).

2. M. Matsuura, N. Kishi, and T. Miki, "Ultrawideband Wavelength Conversion Using Cascaded SOA-Based Wavelength Converters," J. Lightwave Technol. 25, 38-45 (2007).

3. Poustie, "Highly Integrated InP-based Subsystems for All-optical Processing," in *Optical Fiber Communication Conference (OFC)*, (Optical Society of America 2010), paper OWW1.

4. Q. Wang, T. von Lerber, S. Honkanen, and F. Küppers, "Polarization Independent Clock Recovery Scheme based on Birefringent Resonator," J. Opt. Commun. **28,** 242-247 (2007).

5. G. Contestabile, A. Maruta, S. Sekiguchi, K. Morito, M. Sugawara, and K. Kitayama, "160 Gb/s Cross Gain Modulation in Quantum Dot SOA at 1550 nm," in *Proceedings of the European Conference on Optical Communications (ECOC)*, (Vienna, Austria 2009), paper PD 1.4.

6. G. Contestabile, A. Maruta, S. Sekiguchi, K. Morito, M. Sugawara, and K. Kitayama, "Regenerative Amplification in a Quantum Dot SOA," in *Optical Fiber Communication Conference (OFC)*, (Optical Society of America 2010), paper OMT2.

7. M. Nielsen, B. Olsson, and D. Blumenthal, "Pulse Extinction Ratio Improvement using SPM in an SOA for OTDM Systems Applications," Photon. Tech. Lett. **14,** 245-247 (2002).

8. Tervonen, M. Mattila, W. Weiershausen, T. von Lerber, E. Parsons, H. Chaouch, A. Marculescu, J. Leuthold, and F. Kueppers, "Four-port PON Amplifier with over 8-dB Power Budget Improvement, Negligible ASE Noise, and Supporting 30 dB Dynamic Range," in *Proceedings of the European Conference on Optical Communications (ECOC)*, (Torino, Italy 2010), paper Tu 2.2-5.

9. V. Grigoryan, M. Shin, P. Devgan, J. Lasri, and P. Kumar, "SOA-Based Regenerative Amplification of Phase-Noise-Degraded DPSK Signals: Dynamic Analysis and Demonstration," J. Lightw. Technol. **24,** 135-142 (2006).

10. P. Johannisson, G. Adolfsson, and M. Karlsson, "Suppression of phase error in differential phase-shift keying data by amplitude regeneration," Optics Letters **31,** 1385-1387 (2006).

11. T. Vivero, N. Calabretta, I. Tafur Monroy, G. Kassar, F. Ohman, K. Yvind, A. Gonzalez,-Marcos, and J. Mork, “2R-Regeneration in a monolithically integrated four-section SOA-EA chip,” Optics Communications **282,** 117-121 (2009).

12. D. Wolfson, P. Hansen, A. Kloch, T. Fjelde, C. Janz, A. Coquelin, I. Guillemot, F. Gaborit, F. Poingt, and M. Renaud, “All-optical 2R regeneration at 40 Gbit/s in an SOA-based Mach-Zehnder interferometer,” in *Optical Fiber Communication Conference (OFC)*, (Optical Society of America 1999), paper PD36.

13. E. Parsons, H. Chaouch, F. Küppers, T. von Lerber, M. Mattila, W. Weiershausen, A. Tervonen, J.-Y. Yang, and A. Willner, “Photonic Balancing in DPSK Detection Using Pulse Collision in a Semiconductor Optical Amplifier,” in *Proceedings of the European Conference on Optical Communications (ECOC)*, (Vienna, Austria 2009), paper 2.2.5.

14. Gnauck and P. Winzer, “Optical Phase-Shift-Keyed Transmission,” J. Lightw. Technol. **23,** 115-130 (2005).

15. M. Schwartz, W. Bennett, and S. Stein, *Communication Systems and Techniques,* (IEEE Press 1996), Chap 7.

16. H. Chaouch, E. Parsons, and F. Kueppers, "BER Improvement for RZ-DPSK Receivers Using Saturated Asymmetric Filtering," in *Optical Fiber*

Communication Conference, OSA Technical Digest (CD) (Optical Society of America, 2010), paper OTuN2.

17. P. Mamyshev, "All-Optical Data Regeneration Based on Self-Phase Modulation Effect," in *Proceedings of the European Conference on Optical Communications (ECOC)*, (Madrid, 1998), pp. 475-476.

CHAPTER 4

SOA-BASED MAMYSHEV-TYPE REGENERATION, TOWARDS ALL-OPTICAL ERROR CORRECTION

4.1 INTRODUCTION

Mamyshev-type regeneration [1] is one of the first fiber-based all-optical regeneration techniques [2,3,4] for noisy return to zero (RZ) signals. Its simple yet elegant concept lies in a basic property of propagating signals inside highly nonlinear fibers: spectral broadening due to self-phase modulation (SPM).

When noisy ones and zeros enter the HNLF, they experience different nonlinear impacts yielding different spectral responses. The ones' high intensity changes significantly the local refractive index causing self phase modulation and as a consequence the broadening of their spectrum. The zeros' low power on the other hand, prevents any major spectral modification.

Fig. 1 illustrates these two different responses. Linear decomposition of the signal spectrum into ones and zeros' spectra is considered and the resulting transfer function after passing through the detuned narrow filter is presented. The black and red dashed arrows represent the signal tones equally separated by the optical modulation frequency.

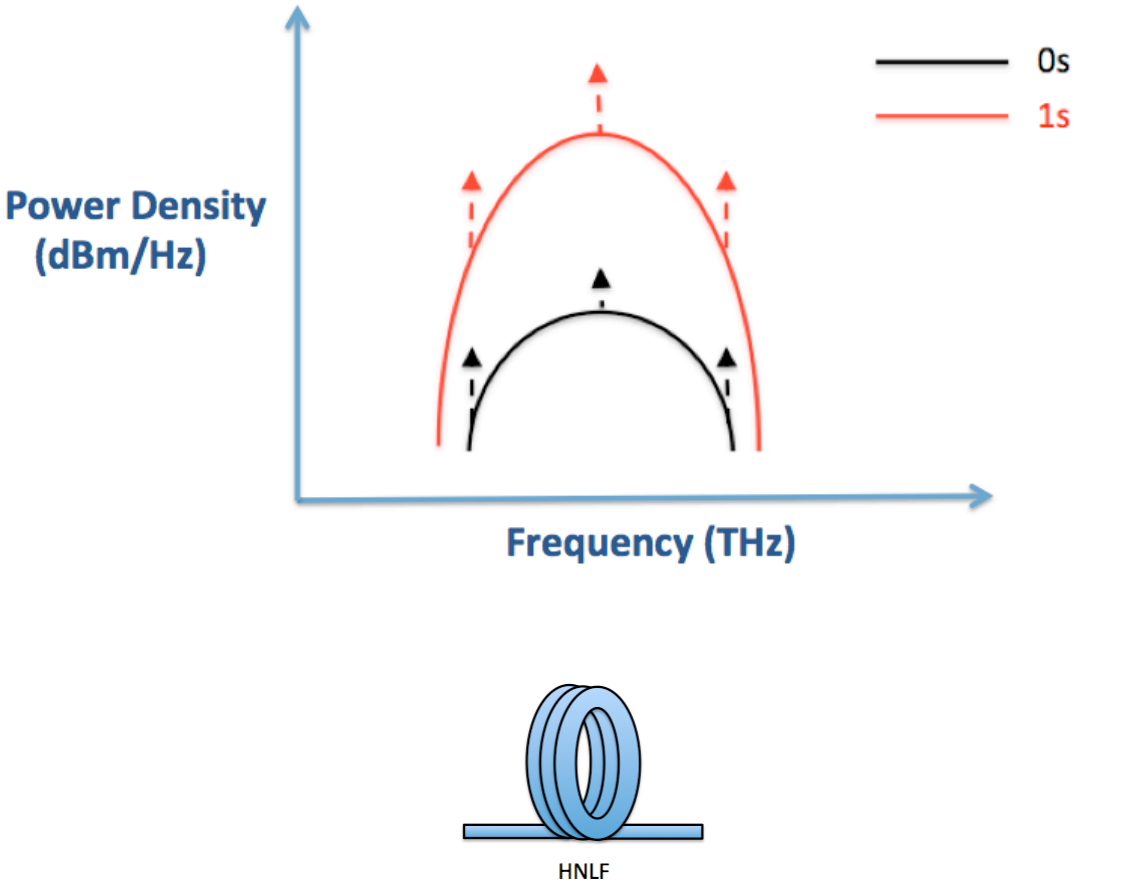
Power Density
(dBm/Hz)
Frequency (THz)
0s
1s
HNLF
Power Density
(dBm/Hz)
Frequency (THz)
0s
1s
Filter

(a)

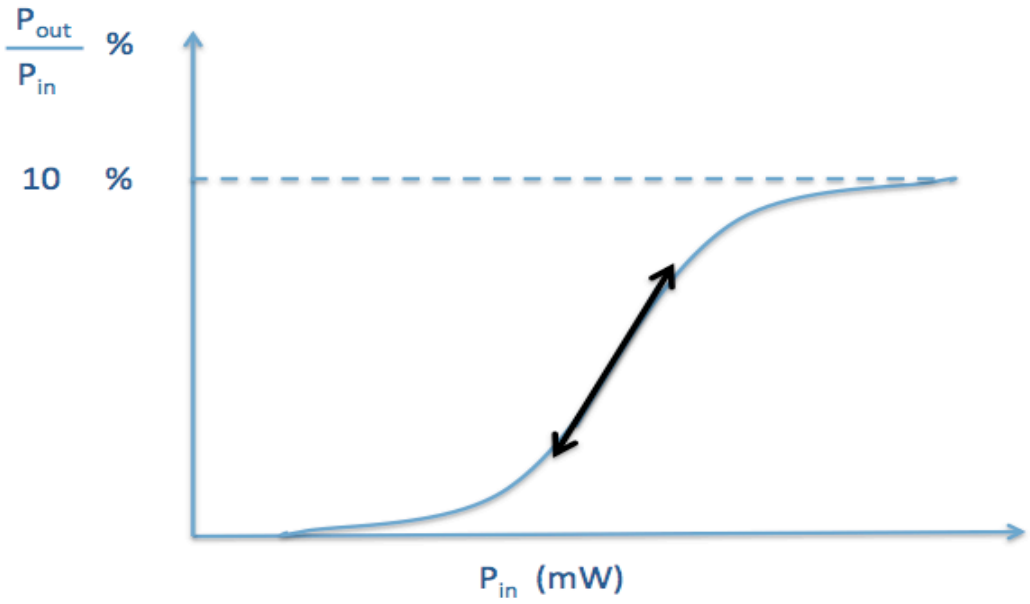

(b)

Fig. 1. Ones and zeros spectra after the HNLF (a) and resulting power transfer function after the detuned narrow filter (b).

A drawback of using a narrow filter is the severe power loss at the regenerator's output. Fig. 1 (b) shows qualitatively a typical optical power transfer function for a fiber-based regenerator. In the Mamyshev-type, an approximate 10 dB power loss has to be compensated for by means of optical amplification. Fiber-based 2R systems however, require the re-amplification of the signal to take place before the re-shaping stage due to the intrinsic amplifier's signal to noise ratio degradation (described by the noise figure).

In order to address this main limitation, we present an SOA-based alternative. The SOA is highly saturated and works in the counter-propagating pulses configuration [5,6]. These last two operation conditions provide the following advantages:

- A high saturation output power

- A strongly broadened spectrum
- A highly asymmetric spectrum [5,8]
- Photonic balancing [6,7] (making the ones and zeros see the same saturated gain)

In the following discussion, we present in section 2 the experimental results obtained with a 20 GHz-bandwidth fiber Bragg grating (FBG) tunable filter. In section 3, we provide a numerical optimization of the filter's detuning and bandwidth.

4.2 EXPERIMENTAL SETUP & RESULTS

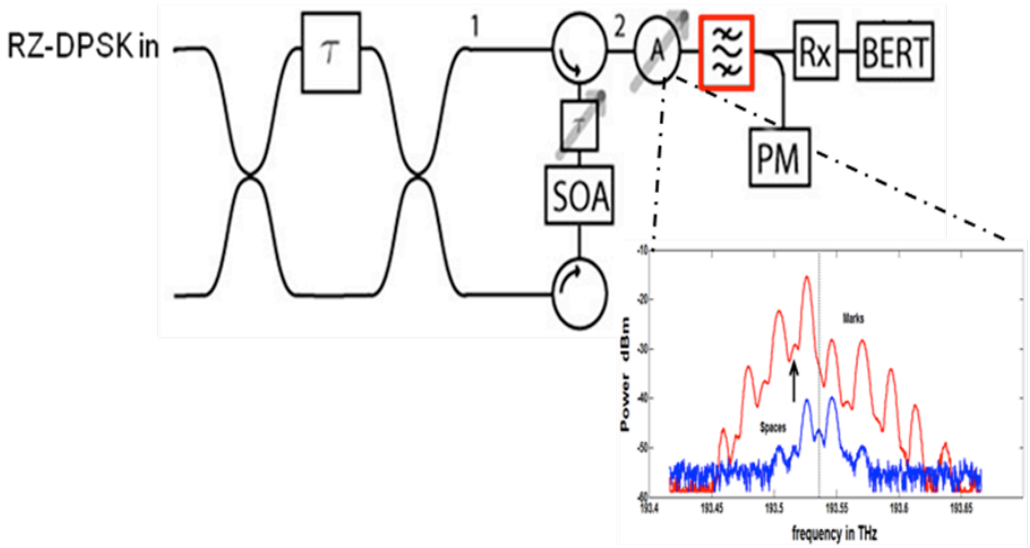

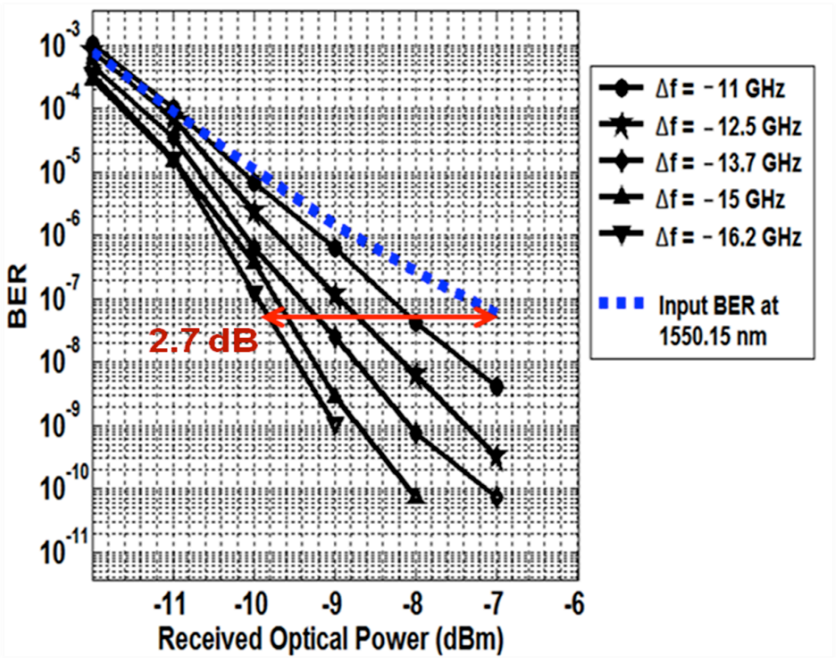

Fig. 2. Experimental Setup and measured BER curves for different filter shifts and receiver input powers. The SOA is operated in the colliding-pulses configuration. The ones asymmetric broadened spectrum is also shown.

The receiver setup is shown in Fig. 2. A 10.7 Gbit/s phase-noise degraded RZ-DBPSK signal is demodulated into two logically opposite amplitude-modulated (AM) signals using a Mach-Zehnder interferometer (MZI). A variable delay line is used to ensure that the collision between a given one and its logically opposite zero occurs exactly at the SOA by matching the length of one MZI output arm to the other [7,8]. Circulators are also used to separate the signals entering from those leaving the SOA. Finally, we connect one arbitrary SOA output arm to an optical attenuator followed by the 20 GHz-bandwidth, first order, Gaussian-shaped FBG filter detuned from the center signal wavelength. This filter is located directly in front of the receiver and is enclosed in a red square in Fig. 2.

A 15 GHz-bandwidth lightwave converter (Rx) detects the detuned filter's optical output signal. The resulting electrical RF signal is analyzed using a bit error ratio tester (BERT). To obtain a reference signal, the variable attenuator followed by a centered filter (at 1550.15 nm) is connected directly at point 1, bypassing the SOA.

When connecting at point 2, we measure the BER evolution with respect to the receiver's optical input power for various filter detuning values. The optimum filter position is found at 1550.28 nm, -16 GHz distant from the 1550.15 nm central wavelength. In this optimal configuration, a 2.7 dB receiver sensitivity improvement is achieved for targeted BERs $\leq 6\times10^{-8}$ as indicated in Fig. 2. Inside the saturated SOA, two fast processes take place:

First, thanks to the counter-propagating pulses configuration, the SOA's saturated gain prevents the amplification of the zeros.

Second, SPM imposes a frequency chirp on the ones shifting the lower frequency components towards their leading edge. They deplete the gain medium first, and experience more gain than the higher frequency components which are present in the trailing edge.

These two processes induce a signal power transfer towards red-shifted wavelengths while the noise power, mainly in the zeros after demodulation [9], remains centered at 1550.15 nm with no significant broadening.

In these conditions, our red-shifted filter provides an error-free signal (BER $\leq 10^{-9}$) when the receiver's optical power is greater than -9 dBm.

4.3 NUMERICAL OPTIMIZATION OF THE DETUNED FILTER

In Section 2, we experimentally varied the filter's central frequency and recorded the BER evolution while keeping the filter's bandwidth constant. One can convincingly argue that the filter's bandwidth itself can significantly influence the quality of the output signal.

In the following discussion we provide the results of numerical simulations in which the filter's bandwidth is also varied. *Optisystem* simulation software offers the possibility to use the SOA in its counter-propagating pulses configuration and was therefore chosen to carry out this optimization.

In our simulation, a 40 Gbit/s RZ-DBPSK signal is generated with a fixed -10 dBm optical power. Three white noise power-levels, applied over the same bandwidth as the

signal's, are separately considered: -22 dBm, -17 dBm, and -10 dBm. The filter under interest is a first order, Gaussian-shaped optical filter. In each iteration, a unique combination of the filter's bandwidth and detuning is considered and the corresponding Q-factor and BER estimates are recorded. Finally, 1024 bits are generated and transmitted through the system providing a good compromise between estimation precision and simulation time [10,11]. Finally a Chi-Squared BER extrapolation method was used to obtain the estimates.

The results are sketched in the form of contour plots and presented below. In Fig. 3, the Q-factor improvement as compared to the back-to-back case (when connecting at point 1 in Fig. 2) is plotted for the three noise power-levels' scenarios. In Fig. 4, BER estimates based on an averaged Chi-squared extrapolation are given.

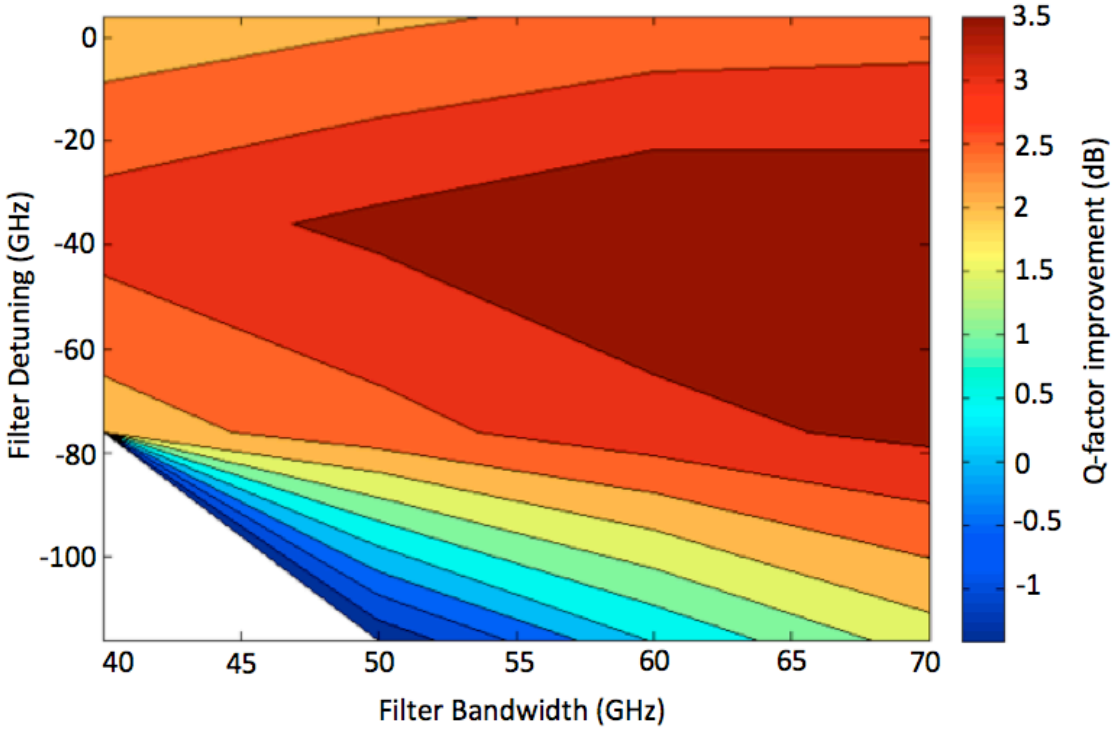

(a)

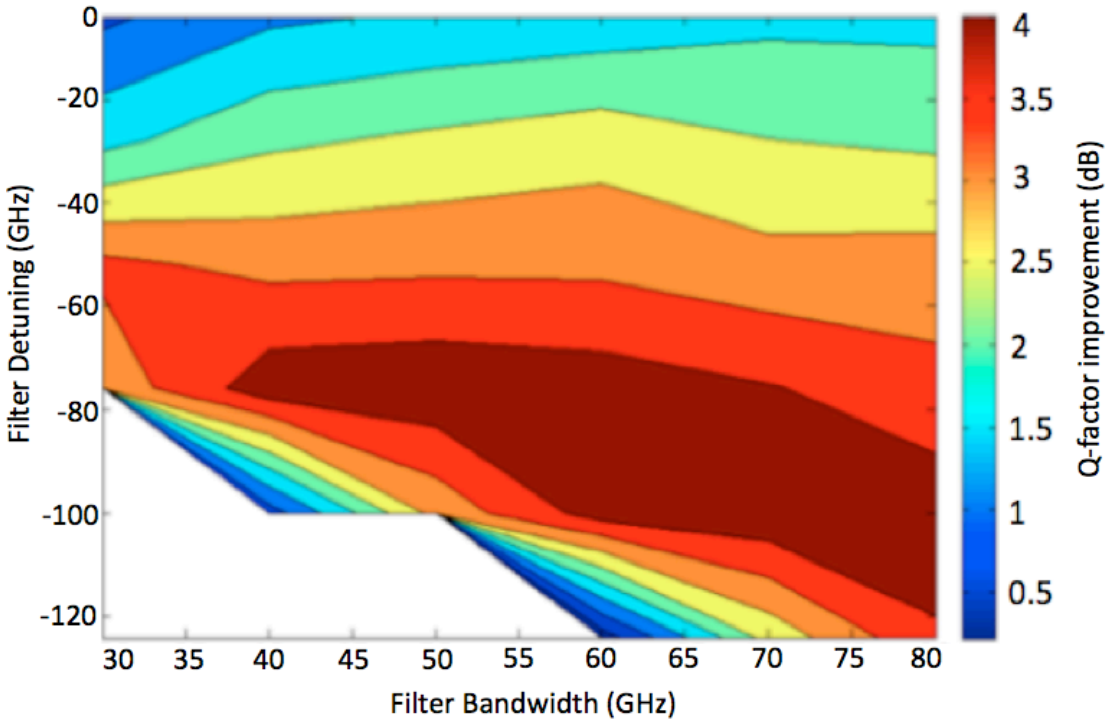

(b)

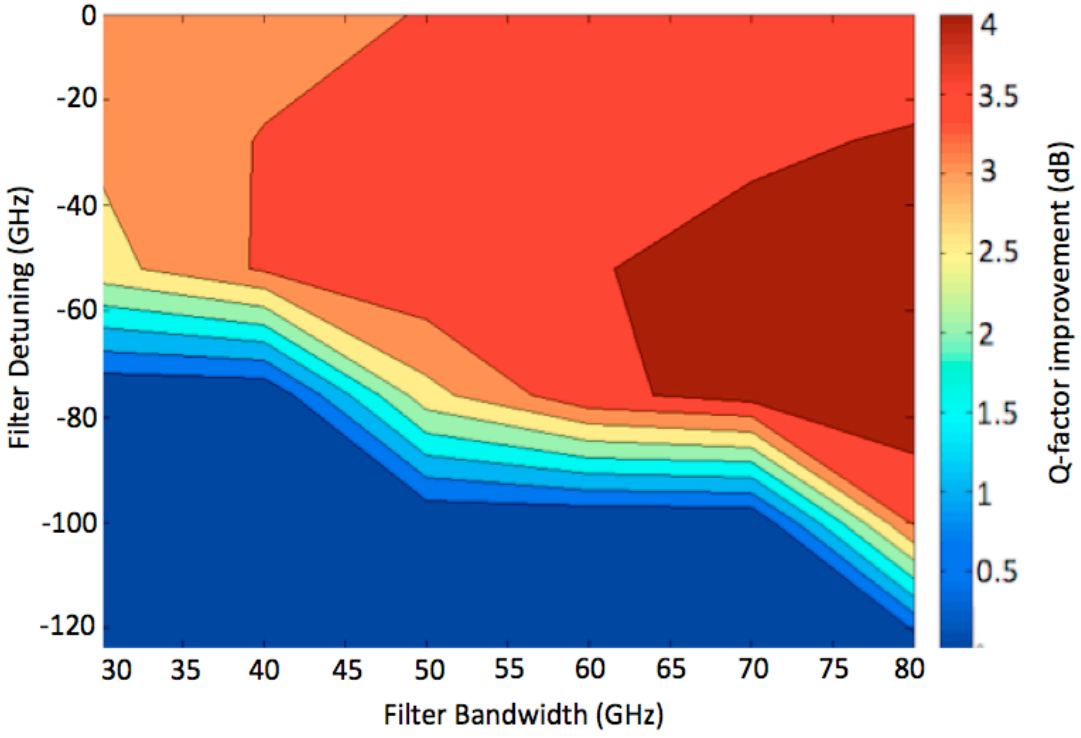

(c)

Fig. 3. Q-factor improvement (in dB) contour plots vs filter detuning and bandwidth. The (a), (b), (c) scenarios correspond to a noise power of -22 dBm, -17 dBm, and -10 dBm respectively. The signal power is maintained at -10 dBm in all cases.The improvement is calculated as compared to the back-to-back Q-factor.

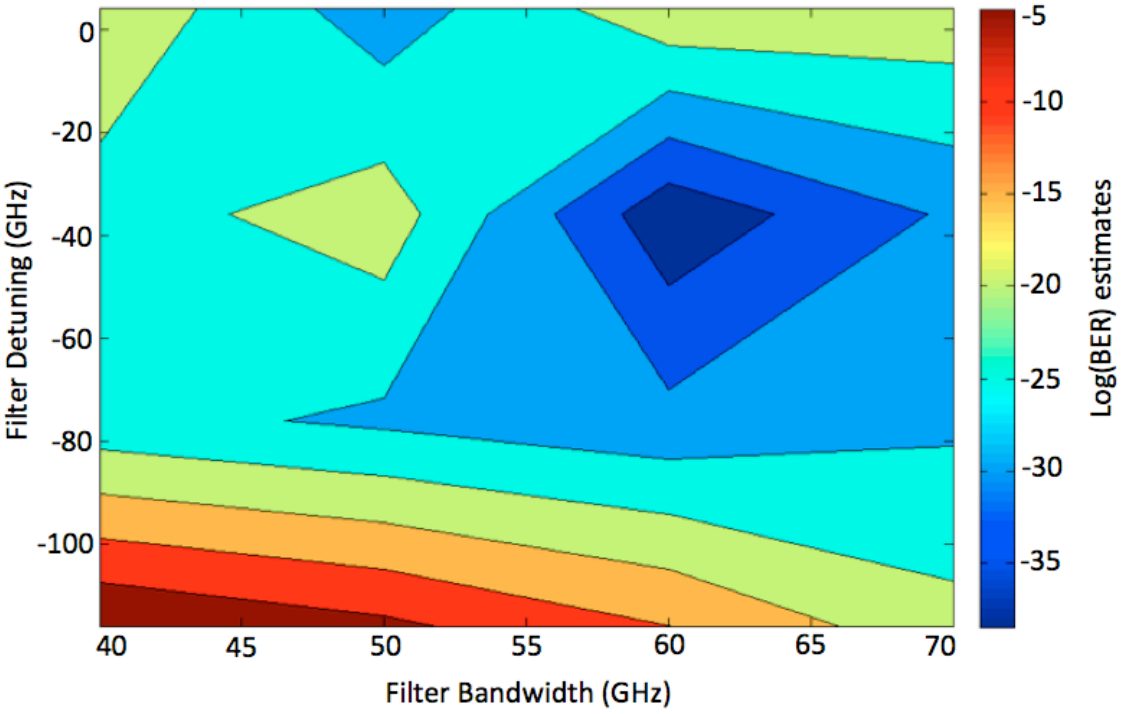
Filter Detuning (GHz)
0
-20
-40
-60
-80
-100
40
45
50
55
60
65
70
Filter Bandwidth (GHz)
-5
-10
-15
-20
-25
-30
-35
Log(BER) estimates

(a)

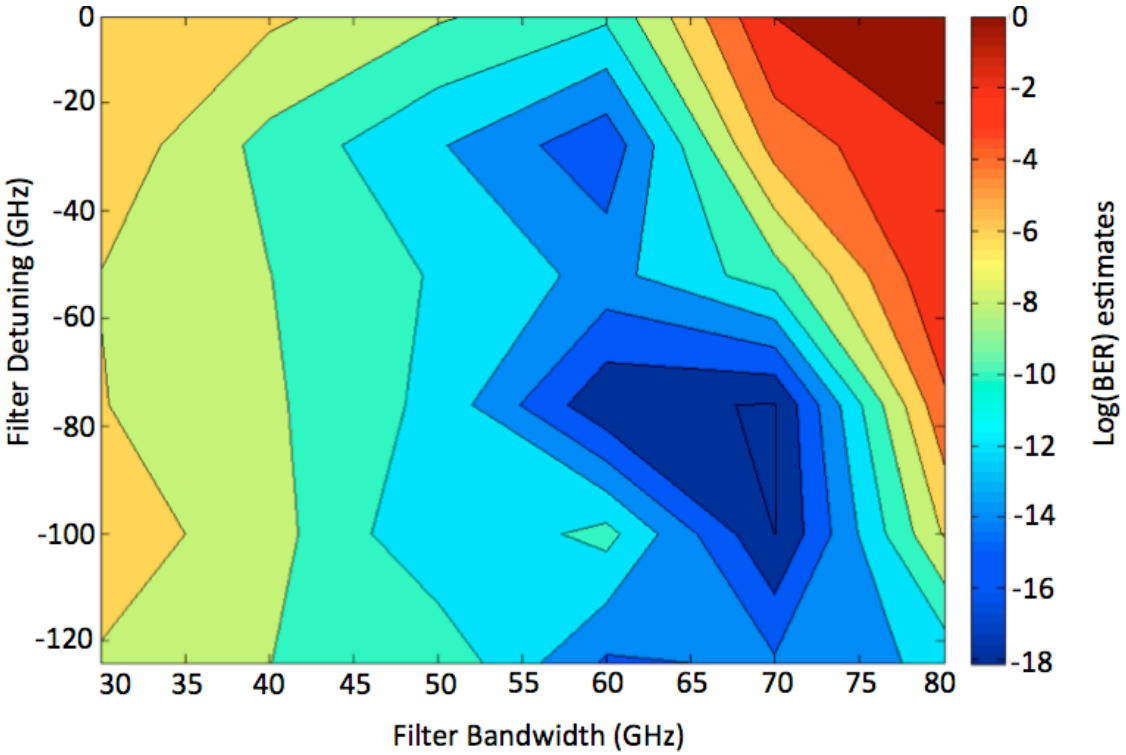
Filter Detuning (GHz)
0
-20
-40
-60
-80
-100
-120
30
35
40
45
50
55
60
65
70
75
80
Filter Bandwidth (GHz)
0
-2
-4
-6
-8
-10
-12
-14
-16
-18
Log(BER) estimates

(b)

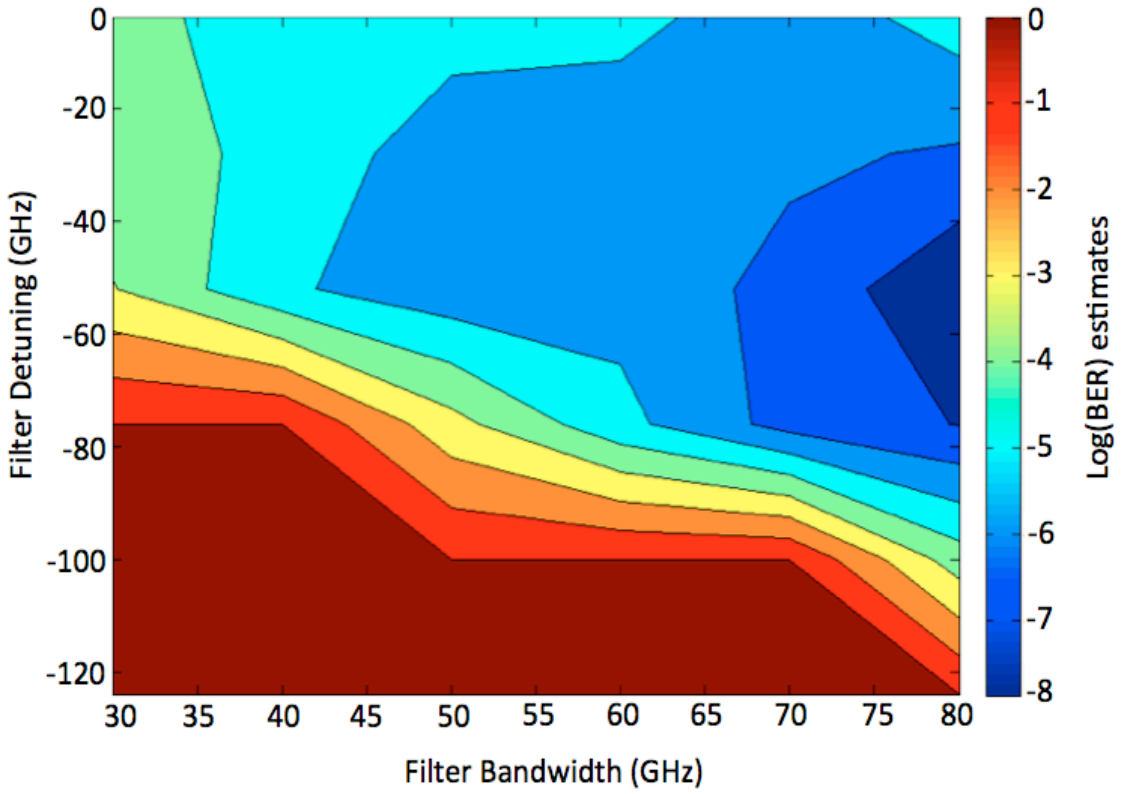

(c)

Fig. 4. Log (BER) estimates contour plots vs filter detuning and bandwidth. The (a), (b), (c) scenarios correspond to a noise power of -22 dBm, -17 dBm, and -10 dBm respectively. The signal power is maintained at -10 dBm in all cases. The averages Chi-Squared BER extrapolation method is used to obtain the estimates. For the back-to-back case the estimated BERs are 10-8, 10-3 and ½ for figures (a), (b), (c) respectively.

Note that the estimated BERs for the back-to-back case in Fig. 4 (a), (b), (c) are 10^{-8}, 10^{-3} and ½ respectively.

Additionally, due to the relatively low noise power coupled to the signal (-22 dBm and -17 dBm), the BER estimates given in Fig 4 (a), and (b) are excessively low and therefore unrealistic. Nevertheless, the trends they display are still of interest since they are in agreement with the Q-factor best-performance ranges, presented in Fig. 3 (a), and (b).

Three fundamental trends can be seen in the above figures:

A) For all three cases, maximum Q-factor improvement (approximately 4 dB) and minimum BER estimates are obtained when the filter is red-shifted. This conclusion confirms our experimental results and can be easily explained by the same arguments as those presented in section 2.

B) When increasing the noise power from -22 dBm to -17 dBm (remaining, however, significantly below the -10 dBm signal power) a deeper red-shift is needed to reach the optimum performance. A minimum filter bandwidth of 45 GHz is furthermore sufficient. In this case, an increase in noise power directly translates into higher amplitude in demodulated zeros that start to experience spectral broadening as well. A larger red-shift is therefore required to filter out the zeros while still selecting the signal.

C) When the signal and noise power are comparable (-10 dBm for both) a smaller red-shift and a significantly wider filter are required. While this can seem in contradiction with the second observation, one has to remember that ones and zeros are present at the same time inside the SOA and deplete equivalently the gain medium when having comparable powers. As a consequence, their respective spectra start overlapping significantly in the red-wavelength zone. Further-shifting the filter is in this case useless since we would start filtering out the signal itself. Additionally, because there is no spectral differentiation between ones and zeroes, a narrow filter cannot be used anymore and a larger bandwidth that enables the selection of more power in the output signal becomes necessary.

These three trends are represented in the spectral domain in Fig. 5 where the optimum filter bandwidth and detuning are qualitatively shown.

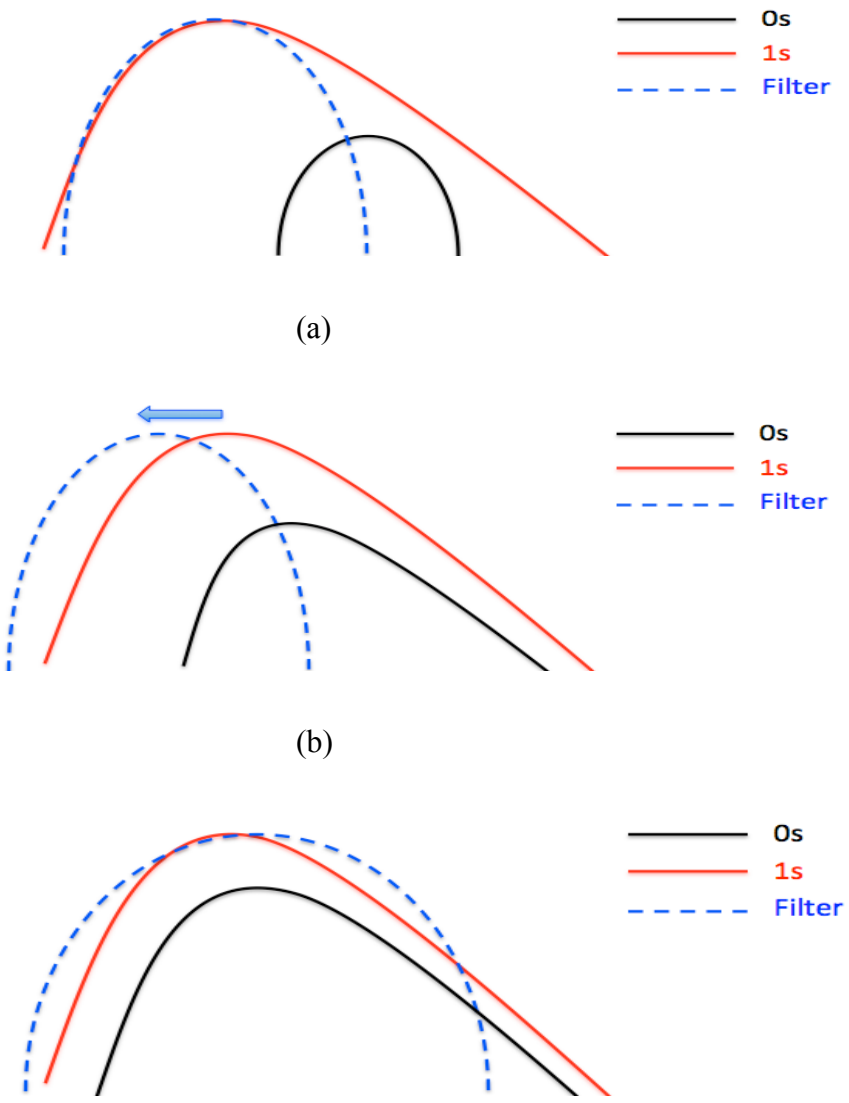

Fig. 5. Qualitative representation of the optimum filter detuning and bandwidth for the three considered noise powers. The (a), (b), (c) figures correspond to the A, B, C scenarios descibed above.

4.4 Conclusion

In this chapter, we showed how a saturated SOA, working in the colliding-pulses configuration, can be used as a better alternative for a Mamyshev regeneration type. We demonstrated a 4 dB improvement in the Q-factor compared to the back-to-back case. For optimum filtering conditions, we detected an almost error free signal for all three noise power-levels. Finally, we explained how the noise power affects the detuning and bandwidth of the filter.

REFERENCES

1. P. Mamyshev, "All-Optical Data Regeneration Based on Self-Phase Modulation Effect," *in Proceedings of the European Conference on Optical Communications (ECOC)*, (Madrid, 1998), pp. 475-476.
2. J. K. Lucek and K. Smith, "All-optical signal regenerator," Opt. Lett. 18, 1226-1228 (1993)
3. P. Petropoulos, T. M. Monro, W. Belardi, K. Furusawa, J. H. Lee, and D. J. Richardson, "2*R*-regenerative all-optical switch based on a highly nonlinear holey fiber," Opt. Lett. 26, 1233-1235 (2001).
4. J. Yu and P. Jeppesen, "Simultaneous All-Optical Demultiplexing and Regeneration Based on Self-Phase and Cross-Phase Modulation in a Dispersion Shifted Fiber, " J. Lightwave Technol. 19, 941- (2001).
5. H. Chaouch, E. Parsons, A. Tervonen, M. Mattila, W. Weiershausen, T. von Lerber, S. Honkanen, J.-Y. Yang, A.E. Willner, F. Küppers. "All-optical processing of RZ-DPSK signals using counter-propagating pulses in a saturated SOA," Optics Communications 284, 2576-2580 (2011).
6. F. Kueppers, E. Parsons, H. Chaouch, W. Weiershausen, M. Mattila, A. Tervonen, T. von Lerber, "Photonic balancing and its application in optical receivers and regenerators for fiber-optic systems," Photonics West, San Francisco, CA, USA, Proc. SPIE, Vol.7621, paper 7621-9 (2010).
7. E. Parsons, H. Chaouch, F. Küppers, T. von Lerber, M. Mattila, W. Weiershausen, A. Tervonen, J.-Y Yang, and A. Willner. "Photonic Balancing in DPSK Detection Using Pulse Collision in a Semiconductor Optical Amplifier," *in*

Proceedings of the European Conference on Optical Communication (ECOC), (Vienna, 2009), pp. Tu 2.2-5.

8. H. Chaouch, E. Parsons, F. Kueppers, "BER Improvement for RZ-DPSK Receivers Using Saturated Asymmetric Filtering," in Optical Fiber Communication Conference and Exposition and The National Fiber Optic Engineers Conference, Technical Digest (CD) (Optical Society of America, 2010), paper OTuN2.
9. P. Johannisson, G. Adolfsson, M. Karlsson, "Suppression of phase error in differential phase-shift keying data by amplitude regeneration," Opt. Lett. 31, 1385-1387 (2006).
10. H. Chaouch, F. Kueppers, S. Vorbeck, M. Schneiders, "Serial 100 Gbit/s PM-RZ-DQPSK transmission in the presence of perturbations from lower data rate neighboring channels," Photonics West, San Francisco, CA, USA, Proc. SPIE, Vol.6721, paper 7621-16 (2010).
11. H. Chaouch, C. Gonschior, K.-F. Klein, S. Vorbeck, M. Schneiders, W. Weiershausen, F. Küppers, "Numerical Analysis and System Optimization for 100 Gbit/s Carrier Ethernet Serial Modulation Formats," Optics Communications 283, 2333-2338 (2010).

REFERENCES

- G. Lehmann, R.H. Derksen, C. Schubert, M. Winter, "100 Gigabit Ethernet Transmission - Physical Layer Issues," in: Optical Fiber Communication Conference, Optical Society of America, 2007. p. OThD5.

- E. Lach, K. Schuh, B. Junginger, G. Veith, J. Lutz, M. Möller, "Challenges for 100 Gbit/s ETDM Transmission and Implementation," in: Optical Fiber Communication Conference, Optical Society of America, 2007. p. OWE1.

- P. A. Humblet and M. Azizoglu, "On the bit error rate of lightwave systems with optical amplifiers," J. Lightwave Technol. 9 (1991) 1576.

- B. Slater, S Boscolo, T Broderick, S.K. Turitsyn, R. Freund, L. Molle, C. Caspar, J. Schwartz, and S. Barnes, "Performance analysis of 20Gb/s RZ-DPSK non-slope matched transoceanic submarine links," Opt. Express 15 (2007) 10999.

- N. S. Bergano, F. W. Kerfoot, and C. R. Davidson, "Margin measuremnets in optical amplifier systems," IEEE Photon. Technol. Lett. 5 (1993) 304.

- G. Bosco and P. Poggiolini, "On the Q factor inaccuracy in the performance analysis of optical direct-detection DPSK systems," IEEE Photonic. Technol. Lett. 16 (2004) 665.

- E.G. Shapiro, M.P. Fedoruk, S.K Turitsyn, "Direct modelling of error statistics at 40 Gbit/s rate in SMF/DCF link with strong bit overlapping," Electron. Lett. 40 (2004) 1436.

- D. Breuer, F. Küppers, A. Mattheus, E.G. Shapiro, I. Gabitov, S.K. Turitsyn, "Symmetrical dispersion compensation for standard monomode-fiber-based communication systems with large amplifier spacing," Opt. Lett. 22 (1997) 982.

- D. Breuer, K. Jürgensen, F. Küppers, A. Mattheus, I. Gabitov, S.K. Turitsyn, "Optimal schemes for dispersion compensation of standard monomode fiber based links," Opt. Commun," 140 (1997) 15.

- H. Wernz, S. Herbst, S. Bayer, H. Griesser, E. Martins, C. Fürst, B. Koch, R. Noe, A. Ehrhardt, L. Schürer, S. Vorbeck, M. Schneiders, D. Breuer, R.-P. Braun, "Nonlinear behaviour of 112 Gb/s polarisation-multiplexed RZ-DQPSK with direct detection in a 630 km field trial," in Proc. of 35th *European Conference on Optical Communication (ECOC 2009), Vienna, Austria, Tu 3.4-3 (2009).*

- S. Xiao and A.M Weiner, "4-user, ~ 3GHz-spaced Sub-Carrier Multiplexing (SCM) using optical direct-detection via hyperfine WDM," IEEE Photonic. Technol. Lett. 17 (2005) 2218.

- M.C. Jeruchim, P. Balaban, K.S. Shanmugan, "Simulation of Communication Systems," *Plenum Press*, New York / London (1994).

- M.C. Jeruchim "Techniques for Estimating the Bit Error Rate in the Simulation of Digital Communication Systems," *IEEE J. Select. Areas Commun*., vol. 2, no. 1, pp. 153-170 (1984).

- H. Wernz, S. Herbst, S. Bayer, H. Griesser, E. Martins, C. Fürst, B. Koch, R. Noe, A. Ehrhardt, L. Schürer, S. Vorbeck, M. Schneiders, D. Breuer, R.-P. Braun, "Nonlinear Behaviour of 112Gb/s Polarization Multiplexed RZ-DQPSK with Direct Detection in a 630 km Field Trial," in Proc. of 35th *European Conference on Optical Communication (ECOC 2009). Vienna, Austria, Mo 3.4.3 (2009).*

- M. N. Islam *et al.*"Cross-phase modulation in optical fibers," Opt. Lett. 12 (8), 625 (1987).

- G. P. Agrawal, *Nonlinear Fiber Optics*, 4th edn., Academic Press, New York (2006).

- C. W. Thiel, "Four-wave mixing and its applications," http://www.physics.montana.edu/students/thiel/docs/FWMixing.pdf

- Slavik, R. *et al.* "All-optical phase and amplitude regenerator for next-generation telecommunications systms," *Nature Photon.* **4,** 690–695 (2010).

- M. Matsuura, N. Kishi, and T. Miki, "Ultrawideband Wavelength Conversion Using Cascaded SOA-Based Wavelength Converters," J. Lightwave Technol. 25, 38-45 (2007).

- Poustie, "Highly Integrated InP-based Subsystems for All-optical Processing," in *Optical Fiber Communication Conference (OFC)*, (Optical Society of America 2010), paper OWW1.

- Q. Wang, T. von Lerber, S. Honkanen, and F. Küppers, "Polarization Independent Clock Recovery Scheme based on Birefringent Resonator," J. Opt. Commun. **28,** 242-247 (2007).

- G. Contestabile, A. Maruta, S. Sekiguchi, K. Morito, M. Sugawara, and K. Kitayama, "160 Gb/s Cross Gain Modulation in Quantum Dot SOA at 1550 nm," in *Proceedings of the European Conference on Optical Communications (ECOC)*, (Vienna, Austria 2009), paper PD 1.4.

- G. Contestabile, A. Maruta, S. Sekiguchi, K. Morito, M. Sugawara, and K. Kitayama, "Regenerative Amplification in a Quantum Dot SOA," in *Optical*

Fiber Communication Conference (OFC), (Optical Society of America 2010), paper OMT2.

- M. Nielsen, B. Olsson, and D. Blumenthal, "Pulse Extinction Ratio Improvement using SPM in an SOA for OTDM Systems Applications," Photon. Tech. Lett. **14,** 245-247 (2002).

- Tervonen, M. Mattila, W. Weiershausen, T. von Lerber, E. Parsons, H. Chaouch, A. Marculescu, J. Leuthold, and F. Kueppers, "Four-port PON Amplifier with over 8-dB Power Budget Improvement, Negligible ASE Noise, and Supporting 30 dB Dynamic Range," in *Proceedings of the European Conference on Optical Communications (ECOC)*, (Torino, Italy 2010), paper Tu 2.2-5.

- V. Grigoryan, M. Shin, P. Devgan, J. Lasri, and P. Kumar, "SOA-Based Regenerative Amplification of Phase-Noise-Degraded DPSK Signals: Dynamic Analysis and Demonstration," J. Lightw. Technol. **24,** 135-142 (2006).

- P. Johannisson, G. Adolfsson, and M. Karlsson, "Suppression of phase error in differential phase-shift keying data by amplitude regeneration," Optics Letters **31,** 1385-1387 (2006).

- T. Vivero, N. Calabretta, I. Tafur Monroy, G. Kassar, F. Ohman, K. Yvind, A. Gonzalez,-Marcos, and J. Mork, "2R-Regeneration in a monolithically integrated four-section SOA-EA chip," Optics Communications **282,** 117-121 (2009).

- D. Wolfson, P. Hansen, A. Kloch, T. Fjelde, C. Janz, A. Coquelin, I. Guillemot, F. Gaborit, F. Poingt, and M. Renaud, "All-optical 2R regeneration at 40 Gbit/s in an SOA-based Mach-Zehnder interferometer," in *Optical Fiber Communication Conference (OFC)*, (Optical Society of America 1999), paper PD36.

- E. Parsons, H. Chaouch, F. Küppers, T. von Lerber, M. Mattila, W. Weiershausen, A. Tervonen, J.-Y. Yang, and A. Willner, "Photonic Balancing in DPSK Detection Using Pulse Collision in a Semiconductor Optical Amplifier," in *Proceedings of the European Conference on Optical Communications (ECOC)*, (Vienna, Austria 2009), paper 2.2.5.

- Gnauck and P. Winzer, "Optical Phase-Shift-Keyed Transmission," J. Lightw. Technol. **23,** 115-130 (2005).

- M. Schwartz, W. Bennett, and S. Stein, *Communication Systems and Techniques,* (IEEE Press 1996), Chap 7.

- H. Chaouch, E. Parsons, and F. Kueppers, "BER Improvement for RZ-DPSK Receivers Using Saturated Asymmetric Filtering," in *Optical Fiber*

Communication Conference, OSA Technical Digest (CD) (Optical Society of America, 2010), paper OTuN2.

- P. Mamyshev, "All-Optical Data Regeneration Based on Self-Phase Modulation Effect," in *Proceedings of the European Conference on Optical Communications (ECOC)*, (Madrid, 1998), pp. 475-476.

- J. K. Lucek and K. Smith, "All-optical signal regenerator," Opt. Lett. 18, 1226-1228 (1993)

- P. Petropoulos, T. M. Monro, W. Belardi, K. Furusawa, J. H. Lee, and D. J. Richardson, "2*R*-regenerative all-optical switch based on a highly nonlinear holey fiber," Opt. Lett. 26, 1233-1235 (2001).

- J. Yu and P. Jeppesen, "Simultaneous All-Optical Demultiplexing and Regeneration Based on Self-Phase and Cross-Phase Modulation in a Dispersion Shifted Fiber, " J. Lightwave Technol. 19, 941- (2001).

- H. Chaouch, E. Parsons, A. Tervonen, M. Mattila, W. Weiershausen, T. von Lerber, S. Honkanen, J.-Y. Yang, A.E. Willner, F. Küppers. "All-optical processing of RZ-DPSK signals using counter-propagating pulses in a saturated SOA," Optics Communications 284, 2576-2580 (2011).

- F. Kueppers, E. Parsons, H. Chaouch, W. Weiershausen, M. Mattila, A. Tervonen, T. von Lerber, "Photonic balancing and its application in optical receivers and regenerators for fiber-optic systems," Photonics West, San Francisco, CA, USA, Proc. SPIE, Vol.7621, paper 7621-9 (2010).

- H. Chaouch, F. Kueppers, S. Vorbeck, M. Schneiders, "Serial 100 Gbit/s PM-RZ-DQPSK transmission in the presence of perturbations from lower data rate neighboring channels," Photonics West, San Francisco, CA, USA, Proc. SPIE, Vol.6721, paper 7621-16 (2010).

- H. Chaouch, C. Gonschior, K.-F. Klein, S. Vorbeck, M. Schneiders, W. Weiershausen, F. Küppers, "Numerical Analysis and System Optimization for 100 Gbit/s Carrier Ethernet Serial Modulation Formats," Optics Communications 283, 2333-2338 (2010).